# Modeling of Performance of Diode-Pumped Nd:$YVO_4$ Laser Systems

**by**

**Ehsan Alimohammadian**

A Thesis submitted to the Faculty of Graduate Studies of

The University of Manitoba

in partial fulfilment of the requirements of the degree of

## Master of Science

Department of Electrical and Computer Engineering
University of Manitoba
Winnipeg, Manitoba,Canada

# Abstract

This thesis focuses on numerical study of a longitudinally pumped continuous wave (CW) Nd:$YVO_4$ laser by high power VCSEL modules. Two VCSEL pump modules (6 W and 15 W) were compared. The performance of Nd:YVO4 crystal was found to be better than that of Nd:YAG crystal. Our numerical results indicate that VCSELs can serve as efficient pump sources for the end-pumped CW Nd:YVO4 lasers.

Internal cavity loss ($L_i$) is an important parameter in the modeling and optimization of laser's performance. A new method for the calculation of the $L_i$ for longitudinally pumped lasers was introduced. This method can be conducted without making any changes to the CW laser cavity and it also can be performed faster compared to the widely used method called Findlay-Clay analysis. A successful experiment was conducted to find the $L_i$ based on both methods with good agreement between the two.

# Acknowledgements

First and foremost, I would like to thank my advisor Dr. Arkady Major for his kind support and guidance during my M.Sc. I would also like to thank my colleagues at the University of Manitoba Tanant Waritanant and Reza Akbari. I would like to extend my gratitude to my M.Sc. committee members Dr. Peter Zetner and Dr. Pradeepa Yahampath.

I would also like to thank my uncle and his wife, Majid and Shadi and my friend Mohammed Asefi.

The financial supports from the Natural Sciences and Engineering Research Council of Canada (NSERC), University of Manitoba and Western Economic Diversification Canada are appreciated.

Keeping the bests for the last, I would like thank my parents for all their love and encouragement.

Ehsan Alimohammadian

*To my parents*

# Contents

# List of tables

Table

# List of figures

Figure

# Chapter1

# Introduction

## 1.1 Motivation

An essential part of an engineering design process is modeling and parameterization of a system. Modeling can lead us to optimization of a design.

Let's consider a situation that we have a pump source with known parameters. For designing an optimized continuous wave CW laser, in addition to a mathematical model for longitudinally pumped (CW) lasers, a step by step procedure will be needed. Later on this optimized CW laser can be used as a starting point for making efficient short or ultra short pulse lasers.

VCSELs (vertical cavity surface-emitting lasers) have several advantages compared to the standard edge emitting lasers. To the best of our knowledge VCSELs have not been used as a pump source for longitudinal pumping of CW lasers. Therefore, in this work we numerically investigated applicability of VCSELs to serve as a excitation source in longitudinally pumped continuous wave Nd:$YVO_4$ and Nd:YAG lasers.

In addition, performance of all types of lasers are greatly affected a parameter called internal cavity loss ($L_i$). Although there is already a method that is widely used for the measurement of such losses called Findlay-Clay analysis, it has some disadvantages. These disadvantages led us to propose and demonstrate a new, simpler method for estimation of the intracavity losses $L_i$.

## 1.2 Objectives

In this work a model of longitudinally pumped CW solid state laser will be discussed in details. Besides, physical interpretation of all mathematical terms in the model will be presented. Using this model for an engineering optimized design of a solid-state CW laser is one of the main purposes of this thesis. Additionally, the design process will be used with high power VCSEL modules serving as longitudinal pump sources to design CW Nd:$YVO_4$ and Nd:YAG lasers.

A new method for the measurement of internal losses $L_i$ will be presented. An experiment was conducted to compare the new method with the well-known Findlay-Clay analysis.

## 1.3 Contributions

In this work the following contributions have been made so far:

- A general CW laser design methodology when this process starts with a given pump source was presented.
- The presented methodology was applied for the modeling of a CW Nd:$YVO_4$ laser longitudinally pumped by high power VCSEL modules at 808 nm. It is worth mentioning that Nd:$YVO_4$ and Nd:YAG crystals were compared as possible candidates to be longitudinally pumped by VCSEL modules. In addition, commercially available 6W and 15W VCSEL modules were compared as a pump source for both of the laser crystals. To the best of our knowledge, this is the first time that VCSELs were considered for longitudinal pumping of a CW laser. The results of this work were presented at the Photonics West 2014 conference [1] and published in conference proceedings [2].

- A new method for the internal cavity loss measurement in all longitudinally pumped lasers was introduced. This method is faster and it can be conducted without several realignments of a laser cavity.
- A successful experiment for the measurement of the internal cavity loss parameter was designed and implemented. In this experiment the new method and the Findlay-Clay were implemented and compared.

## 1.4 Outline of the thesis

Main laser engineering concepts used in this thesis will be explained in Chap. 2. Moreover a new device called VCSEL will be described. Chap. 2 starts with a solution of Helmholtz equation for a paraxial wave called Gaussian beam. The main parameters of the Gaussian beam will be discussed in this chapter. Next, a famous model for CW operation of a solid state laser longitudinally pumped by a pump with Gaussian distribution will be explained. Final results of the model are a function called *f* function and an equation for output power as a function of input power and the *f* function. The *f* function shows the intracavity power as a function of a ratio of the pump power to the threshold power. This function can be evaluated for different laser media, different pump and laser beams overlap, and pump distribution.

In addition in Chap.2, a parameter called 10% confocal parameter will be introduced. This parameter will be used in Chap.3 for finding an optimum value for the gain medium length. Final part of Chap.2 is devoted to VCSEL and some of its properties.

In Chap. 3, a step by step methodology for designing an optimized longitudinally pumped CW laser when the parameters of the pump source are known will be discussed. Next, this methodology will be used for designing a longitudinally pumped CW laser.

In Chap. 3, the *f* function defined in previous chapter will be generated for a 4 level gain medium and certain pump distribution with specific laser and pump beams overlap. In this chapter longitudinal pumping of a CW Nd:$YVO_4$ laser by high power VCSEL modules will be numerically modelled for an equal laser and pump beams overlap.

In the numerical model presented in Chap.3, commercially available 6W and 15W VCSEL modules will be studied as potential pump sources and the performance of Nd:$YVO_4$ and Nd:YAG crystals as two possible candidates to be longitudinally pumped by them will be investigated. To the best of our knowledge, this is the first time that VCSELs were considered and analyzed for longitudinal pumping of a CW laser. In addition for both pumps and gain media, the optimum output couplers, slope efficiency, maximum output power and optical-to-optical efficiency were determined.

The selected VCSEL modules have a beam with high divergence. Therefore as it will be discussed in Chap.3 the10% confocal parameter is a useful tool for finding an optimized value for the gain medium length.

In modeling of CW lasers, the losses in the cavity are assigned to two parameters; the loss due to the transmission of an output coupler and a loss introduced by the imperfection of the mirrors called internal cavity loss. In Chap.4 a new method for the measurement of the internal cavity loss parameter will be introduced. This method has some advantages compared to the previous method called Findlay-Clay analysis (explained in Chap.2).

In addition, an experiment was designed to measure internal cavity loss using the new method and the Findlay-Clay method. The new method is based on the model explained in Chap.2. Since the beam distribution of the pump used in the experiment is closer to a top-hat than to a

Gaussian, an *f* function will be generated for the designed CW laser longitudinally pumped with a top-hat beam. Finally, the possible sources of errors in the experiment will be discussed.

Chap.5 of the thesis is assigned to the conclusions and possible future work.

# Chapter2

# Background information

## 2.1 Overview

In this chapter the main concepts which will be used in the next chapters, are reviewed. In addition, a device called VCSEL is briefly explained.

This chapter starts with definition of a Gaussian beam and introducing some of its properties.

Next section starts with describing the rate equations of a laser. This will lead us to the fundamental principles of operation of a CW laser. In section 2.3, a model for CW operation of a laser called Risk model will be explained in detail. In this model laser beam and pump beam are assumed to be Gaussian beams.

Section 2.4 is devoted to modeling of the laser output power and defining efficiencies of a laser in continuous wave regime. These are useful for comparison of CW operation of different lasers.

In section 2.5, an experimental method for finding internal cavity loss, which is an important parameter in modeling of CW lasers, will be explained.

Last section of this chapter is about VCSEL device and its properties.

## 2.2 Gaussian beam

A light with constant properties traveling in free space can be considered as an ideal source for many applications, for example pumping (i.e. excitation) of a laser medium. Considering the wave nature of light, a plane wave can provide this condition for us. When a plane wave travels

the amplitude of field distribution (i.e. $A_0$) stays constant. If the direction of propagation is along the z axis, then a plane wave can be represented as $A_0 e^{-jkz}$. In real situation, however, small transverse variation of optical field distribution will result in the modulation of plane waves. Mathematical representation of a traveling plane wave modulated by an envelope is called a paraxial wave. Paraxial waves in cylindrical coordinates can be represented as follows [3and 4]:

$$U(r,\varphi,z) = U(r,z) = A(r,z)\, e^{-jkz}, \tag{2.1}$$

where $A(r,z)$ is the modulating envelop which depends on position. Here, r is the distance from the z axis in the transverse direction [4]. In the case above an axial symmetry is assumed [4].

An important solution to the Helmholtz equation for a paraxial wave is as follows: [3,4]

$$U(r,z) = A_0 \frac{W_0}{W(z)} \exp[-\frac{r^2}{W^2(z)}]\exp[-jkz - jk\frac{r^2}{2R(z)} + j\zeta(\mathrm{z})\ ], \tag{2.2}$$

where

$$W(z) = W_0\sqrt{1+\left(\frac{z}{z_0}\right)^2}, \tag{2.3}$$

$$R(z) = z\left[1+\left(\frac{z_0}{z}\right)^2\right], \tag{2.4}$$

$$\zeta(\mathrm{z}) = \tan^{-1}\frac{z}{z_0}, \tag{2.5}$$

$$W_0 = \sqrt{\frac{\lambda z_0}{\pi}}, \tag{2.6}$$

and $U(r,z)$is called a Gaussian beam.

In the above equations, $\lambda$ is the wavelength, z is the distance along the direction of propagation of radiation (i.e. axial distance).W (z) represents the beam radius function with respect to z and $W_0$ is called the beam waist radius which is the minimum beam radius of a Gaussian beam. $z_0$ is called the Rayleigh range. The Rayleigh range is a certain distance at which the beam's radius function W(z) increases to $\sqrt{2}W_0$. Figure 2.1 shows a schematic representation of a Gaussian beam and its main parameters. A distance which is twice the Rayleigh range is called the depth of focus or confocal parameter. This is a distance where the beam waist radius stays smaller than the $\sqrt{2}W_0$ [3].

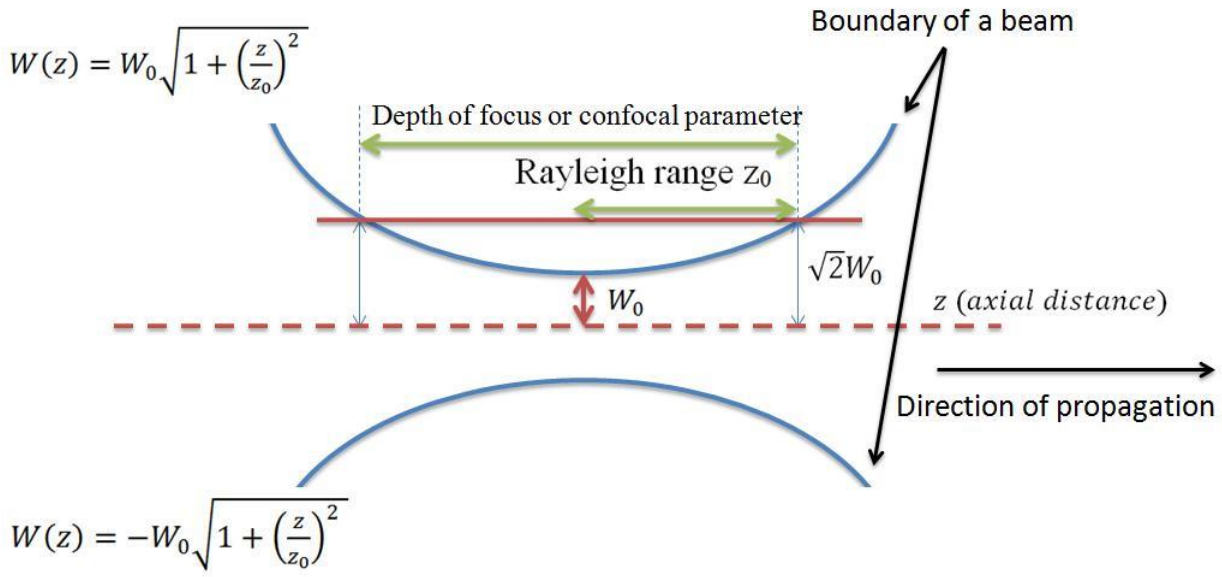


Figure 2.1 Rayleigh range and depth of focus (confocal parameter)

Gaussian beams have several properties which can be obtained from the above equations. In our analysis, the beam waist, depth of focus (or confocal parameter) and beam quality factor ($M^2$) will be used.

### 2.2.1 Beam quality factor ($M^2$)

$M^2$ (reads as "M squared") is a parameter that quantitatively gives us an idea about the quality of a Gaussian beam, i.e. whether it is multimode or not. In practical terms, $M^2$ factor shows divergence of a Gaussian beam.

Considering equation 2.3 in the far field (i.e $z \gg z_0$) for an ideal Gaussian beam by substituting $z_0$ from the equation 2.6, a relation between the angular divergence and the beam spot can be found as follows:

$$W(z) \cong W_0 \frac{\lambda z}{\pi W_0^2} = \theta_0 Z. \tag{2.7}$$

Therefore:

$$\theta_0 = \frac{\lambda}{\pi W_0}, \tag{2.8}$$

where $\theta_0$ is angular divergence of an ideal Gaussian beam profile. It is clear that $2\theta_0$ is the divergence angle of an ideal Gaussian beam [3].Therefore in an ideal Gaussian beam a product of the beam waist and the angular divergence is constant (i.e. $2\theta_0 2W_0 = \frac{4\lambda}{\pi}$).

Mathematically speaking, the $M^2$ shows deviation of a beam under test from an ideal Gaussian beam profile [3]. Therefore, for a beam with the waist of $2W_m$ and the angular divergence of the $2\theta_m$, the $M^2$ factor can be defined as follows [3]:

$$M^2 = \frac{2W_m.2\theta_m}{2W_0.2\theta_0} = \frac{2W_m.2\theta_m}{\frac{4\lambda}{\pi}} = \frac{W_m.\theta_m}{\frac{\lambda}{\pi}}, \tag{2.9}$$

and therefore,

$$\theta_m = \frac{M^2\lambda}{\pi W_m}. \tag{2.10}$$

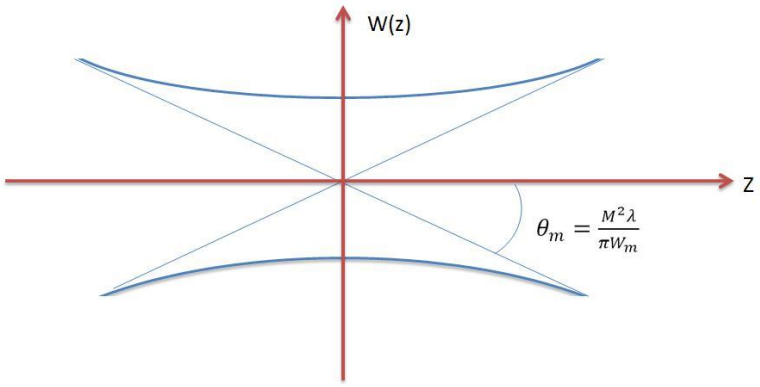


Figure 2.2 Relationship between $\theta_m$, $M^2$, $\lambda$ and $W_m$ [5]

Figure 2.2 shows the angle $\theta_m$ of a propagating Gaussian beam. To see the effect of $M^2$ on a Gaussian beam, three Gaussian beams with different $M^2$ factors were compared. Figure 2.3 shows Gaussian beams emitted by a laser diode with wavelength of 808 nm, emission area of 2.6 mm (i.e. $W_m$=1.3 mm) for different $M^2$ factors. To imagine a real situation, one can consider the center of the laser diode emission area at the origin z=0.

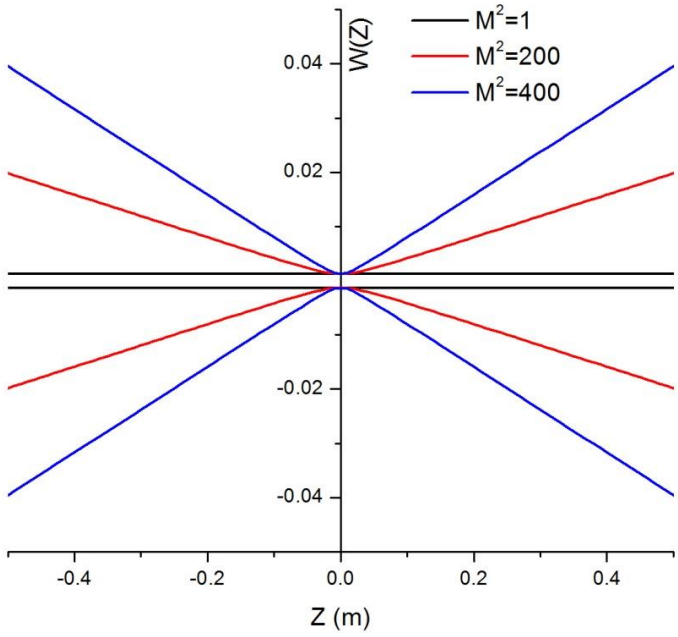


**Figure 2.3 Gaussian beams emitted by a laser diode with wavelength of 808 nm, emission area of 2.6 mm for different $M^2$ factors**

As can be seen in the above graph if the $M^2$ is close to 1, the divergence of the Gaussian beam will be very small. Therefore $M^2$=1 is an ideal case for a Gaussian beam. As the value of the $M^2$ is getting larger the beam diverges faster. This means that it is hard to keep a beam with high $M^2$ focused over a certain distance.

In some datasheets of laser devices such as diodes or VCSELs only numerical aperture (NA), and the size of the emitting area ($2W_0$) are provided. Finding $M^2$ for these devices using provided datasheets (without doing the beam width measurement) requires an equation to relate the numerical aperture and the minimum beam waist.

Considering a relation for numerical aperture $NA = nsin(\theta)$ where n is the refractive index (for propagation of light in the air $n \cong 1$) results in:

$$\theta = sin^{-1}(NA). \tag{2.11}$$

Using Taylor's series first truncation, for small angles we can use $sin^{-1}(\theta) \cong \theta$ approximation, where angle $\theta$ is measured in radians. Therefore, for small angles equation 2.10 can be re-written as follows

$$NA \cong \frac{M^2\lambda}{\pi W_m}. \tag{2.12}$$

However, doing an experiment to find the beam quality through the beam waist measurements would provide more accurate result for $M^2$.

The $M^2$ factor of a laser with a Gaussian beam can be found by measuring the beam's width at different distances along the z axis and then by fitting this data with the following equation:

$$W(z) = W_0\sqrt{1 + \left(\frac{M^2\lambda\, z}{\pi W_m^2}\right)^2}. \tag{2.13}$$

### 2.2.2 Propagation of a Gaussian beam inside a medium

Equation 2.13 can be used if the Gaussian beam propagates in the air. As we know, the light propagates inside a medium with $n > n_{air}$ at a lower speed than that of free space. To take into account this fact, for a propagating light with Gaussian distribution inside a medium, the wavelength should be divided by the refractive index of the medium. Therefore equation 2.13 would become:

$$W(z) = W_0\sqrt{1 + \left(\frac{M^2\frac{\lambda}{n}z}{\pi W_m^2}\right)^2}. \tag{2.14}$$

Considering the propagation of light inside a medium with refractive index of n, equation 2.12 also can be re-written as:

$$NA \cong \frac{M^2 \lambda}{n\pi W_m}. \tag{2.15}$$

### 2.2.3 Depth of focus (in general and our definition of 10%)

In CW regime, a pump is used to make population inversion in a laser gain medium. There are mainly two methods of pumping, called side pumping and end pumping (or longitudinal pumping). In our work, the end pumping will be considered. The main sources of longitudinal pumping are laser diodes. The beam generated by laser diodes is usually modeled as a Gaussian beam. Pump beams have their own $M^2$ regardless of the generated laser beam. Considering the beam divergence of the pump sources, we defined a 10% depth of focus parameter. This is a distance over which the beam waist increases only by 10%. This distance is about 46% of the depth of focus or confocal parameter defined earlier. Figure 4 shows a schematic of a Gaussian beam and the 10% depth of focus parameter.

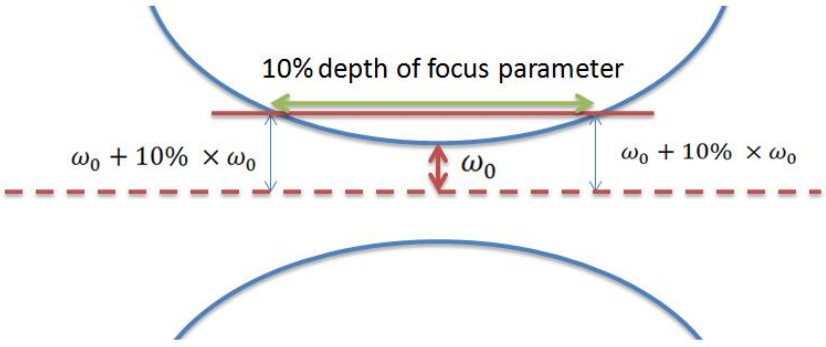


Figure 2.4 10% depth of focus parameter

We can say that over this length the pump beam waist will remain almost constant. In the next chapters, the 10% depth of focus parameter will be used to determine the optimum length for the crystal which will be pumped by a particular pump.

## 2.3 Model of a CW laser

Models of CW lasers presented in articles [6, 7 and 10] are based on rate equations. Therefore we start this section with a brief review of these equations. Then, the Risk model [6] will be explained in more details. The final results of this model are two equations for finding laser's threshold pump power and output power. These equations will be used in the next chapters.

### 2.3.1 Rate equations

Rate equations provide information about population of photons inside of a laser resonator and population of electrons on atomic scale inside a gain medium [3]. These equations will allow us to find mathematical expressions for threshold pump power and steady state operation of a laser in a CW regime. In addition, rate equations also can be used for modeling of the Q-switched lasers [9, 10].

**First equation**

Intuitively, this equation establishes a relation between the total population of electrons in the upper laser level with respect to time, which is affected by electrons generated by the pump as well as by stimulated and spontaneous emission of photons [11].

$$\frac{\partial N}{\partial t} = R_p - WN - \frac{N}{\tau}. \tag{2.16}$$

We have partial derivative due to having a certain pump distribution inside a gain medium [12 and 6]. $\frac{\partial N}{\partial t}$ stands for changes in electron population in the upper laser level with respect to time (i.e. number of electrons in the upper state level at a certain moment). $R_p$ is the number of electrons in the upper state level which were brought by the pump (i.e. excitation) with respect to time (population generated by the pump with respect to time). W is the absorption rate. The product $WN$ represents a number of electrons which are converted into the photons through stimulated emission. And $\frac{N}{\tau}$ stands for a number of electrons which decay to a lower laser level by spontaneous emission, where $\tau$ is the upper state lifetime. As can be seen from the above equation, pump energy increases the population of electrons in the upper laser level ($R_p$) while stimulated emission and spontaneous emission ($WN$ and $\frac{N}{\tau}$, respectively ) decrease their population [11].

**Second equation**

Second rate equation expresses the rate of change in the total number of photons in the cavity with respect to time [11]:

$$\frac{d\phi}{dt} = \int_a WNdV - \frac{\phi}{\tau_c}, \tag{2.17}$$

where $\phi$ is the total number of cavity's photons and $\tau_c$ is the photon's lifetime. $\int_a WNdV$ stands for number of photons generated inside the gain medium due to the stimulated emission. As can be seen, in this expression we have integration over a volume. It is the volume occupied by the laser mode inside the gain medium. It is worth mentioning that the time dependency of this expression is embedded inside the WN product [11].

The term $\frac{\phi}{\tau_c}$ represents the rate with which photons disappear in the cavity due to the losses [11]. In a laser cavity we have two kinds of losses. The first loss is called internal cavity loss which is caused by imperfections of optical elements like mirrors and lenses. This loss is an undesired one and which is always tried to be eliminated from a cavity. The second type of loss is generated due to the transmission of an output coupler. This loss is a desired loss which provides the output laser radiation. Conceptually, by introducing this loss into a cavity we are extracting a fraction of the intracavity power out of the laser cavity.

### 2.3.2 Risk model

In the Risk model described in [6], similar rate equations are used. However, population is defined as a function of spatial coordinates in the gain medium. In addition, the pump and laser distributions are related spatially. That is why this model is considered as a space dependent model [11]. Spatial dependency of electron population N is shown by a cylindrical coordinate system with a fixed angle $\phi$ (i.e. $\phi = 360°$) and variables r and z, which are the radius of a circle (angular coordinate in a cylindrical coordinate system or $\rho$) and distance along the laser axis (longitudinal axis in a cylindrical coordinate system or z), respectively. It is worth mentioning that in the W. P. Risk's article the expressions are written such that the time dependency is not clear but as explained in the previous section the rate equations are a variation of population with respect to time.

**First rate equation**

Figure 2.5 shows a schematic of a laser level system modeled by the Risk. In this model, it has been assumed that the relaxations from $N_3$ to $N_2$ and from $N_1$ to $N_0$ are very fast. Ground level

($N_0$) depletes due to pump distribution and there is a small thermal population in level $N_1$[1]. Having population of electrons in the upper laser level ($N_2$) and the lower level ($N_1$) it can be assumed that we have a two level system.

Equation 2.18 establishes a relation for the unpumped population inversion between the two level system ($\Delta N^0$) which corresponds to a non lasing condition.

$$\Delta N^0 = N_2^0 - N_1^0. \tag{2.18}$$

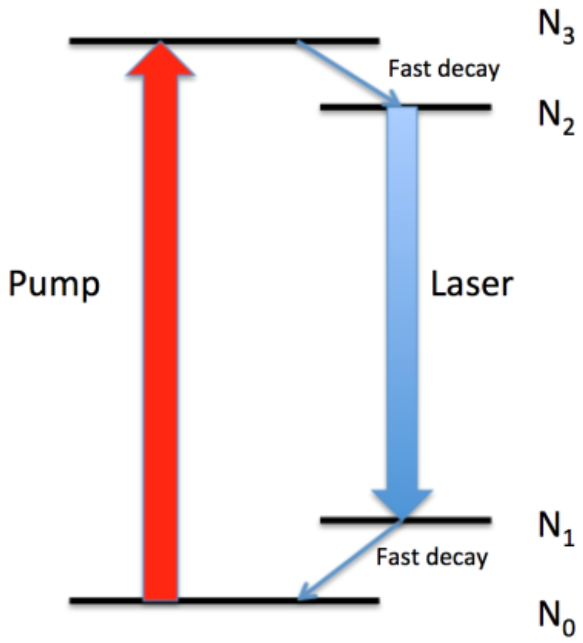


Figure 2.5 Schematic of the laser levels in the Risk model

The first rate equation was written by Risk only for the levels $N_2$ and $N_1$ (equations 2.19 and 2.20 respectively) [6] and steady-state conditions (i.e. $\frac{dN_2(r,z)}{dt} = \frac{dN_1(r,z)}{dt} = 0$) [3]:

[1] Considering thermal population in level $N_1$, makes Risk's model different from a typical 4 level system.[6]

$$\frac{dN_2(r,z)}{dt} = f_2 R r_p(r,z) - \frac{N_2(r,z)-N_2^0}{\tau} - \frac{f_2 c\sigma[N_2(r,z)-N_1(r,z)]}{n}\Phi\phi_0(r,z) = 0, \quad (2.19)$$

$$\frac{dN_1(r,z)}{dt} = -f_1 R r_p(r,z) - \frac{N_1(r,z)-N_1^0}{\tau} + \frac{f_1 c\sigma[N_2(r,z)-N_1(r,z)]}{n}\Phi\phi_0(r,z) = 0. \quad (2.20)$$

Considering a two level system, in the above equations $f_1$ and $f_2$ represent a fraction of the excited electrons in the $N_2$ (upper laser level) and $N_1$ (lower laser level), respectively.

Let's compare equation 2.19 with the first rate equation in section 2.3.1 (i.e. equation 2.16).

We can say that the term $f_2 R r_p(r,z)$ is the fraction of the electrons in the upper laser level ($N_2$) brought to level $N_2$ through pumping with respect to time and spatial pump distribution $r_p(r,z)$. R is the rate of electrons inside the gain medium excited by the pump, i.e. it is the number of absorbed pump photons per unit time. Therefore, $R = \frac{P_p \eta_a}{h\nu_p}$ where $P_p$ is the incident pump power, $h\nu_p$ is the energy of a pump photon, $h$ is the Planck's constant and $\nu_p$ is the pump frequency. $\eta_a$ is the absorption efficiency which is an exponential decaying function

$$\eta_a = 1 - \exp(-\alpha l), \quad (2.21)$$

where $\alpha$ is the pump absorption coefficient which is a function of wavelength, and $l$ is the length of a gain medium (i.e. laser crystal). It is worth mentioning that $P_p \eta_a$ is simply an absorbed pump power.

To take into account the spatial pump distribution, pump is assumed to be a circular Gaussian beam in its fundamental mode. Rewriting equation 2.2 for a circular Gaussian beam which is normalized for $\iiint r_p(r,z)dV = 1$ yields:

$$r_p(r,z) = \frac{2\alpha}{\eta_a \pi w_p^2} \exp(-\frac{2r^2}{w_p^2})\exp(-\alpha z), \quad (2.22)$$

where $w_p$ is the pump beam waist which depends on z coordinate.

It is worth mentioning that in the Risk model only oscillation of the fundamental laser mode inside the cavity was considered.

Comparing equations 2.19 and 2.16, we can say that the term $\frac{N_2(r,z)-N_2^0}{\tau}$ represents the rate of spontaneous emission. The term $N_2(r,z) - N_2^0$ is the effective population in the upper state which is available for spontaneous emission. As before, $\tau$ is the lifetime of the upper manifold. $N_2(r,z)$ is the pumped population inversion and $N_2^0$ is the unpumped population inversion initially residing in the upper laser level.

Considering equations 2.19 and 2.16, we can say that the term $\frac{f_2 c\sigma[N_2(r,z)-N_1(r,z)]}{n}\Phi\phi_0(r,z)$ in the equation 2.19 is represented as the product $WN$ in the equation 2.16. Both of these expressions correspond to the rate of change of population in the upper state which is caused by the stimulated laser emission, where c is the speed of light in the free space and $\sigma$ is the emission cross section of the gain medium at the lasing wavelength. Since the light propagates with slower speed inside the gain medium, the speed of light is divided by the refractive index of the gain medium n. Φ is the total number of laser photons in the cavity with respect to time which can be calculated from $\Phi = \frac{2nlP_L}{ch\nu_L}$, where $P_L$ is the intracavity laser power in one direction. Considering a full round trip in a cavity, $P_L$ should be multiplied by a factor of 2. By dividing the total internal cavity power (i.e. $2P_L$) by the energy of a laser photon (i.e. $\frac{1}{h\nu_L}$) and multiplying it by the time it takes for a laser photon to travel the whole length of the crystal (i.e. $\frac{nl}{c}$), we can find the total

number of laser photons in the cavity with respect to time. Function $\phi_0(r,z)$ is the spatial distribution of the laser photons which is normalized according to the $\iiint \phi_0(r,z)dV = 1$ relation. Risk model assumed that the generated laser beam is a circular Gaussian beam which is a function of space (i.e. in cylindrical coordinates system it is a function of $r,z$) as follows:

$$\phi_0(r,z) = \frac{2}{\pi w_L^2 l}\exp(-\frac{2r^2}{w_L^2}), \tag{2.23}$$

where $w_l$is the generated laser's beam waist which depends on z. [8]

Now let's compare equations 2.20 and 2.16. The term $\frac{f_1 c\sigma[N_2(r,z)-N_1(r,z)]}{n}\Phi\phi_0(r,z)$ represents the rate of change of population of electrons which emitted laser photons by going down to the lower laser level ($N_1$). As can be seen, it is the only expression on the right hand side of equation 2.20 which has a positive sign. This means that it is the only source of electron generation in the lower laser level ($N_1$).

Considering equation 2.18, the term $-f_1 R r_p(r,z)$ is a fraction of the electrons in the lower laser level ($N_1$) with respect to time and spatial pump distribution $r_p(r,z)$, removed from the level $N_1$ by pumping. Similar to equation 2.19, the term$-\frac{N_1(r,z)-N_1^0}{\tau}$ corresponds to the rate of spontaneous emission but for the lower laser level $N_1$. Spontaneous emission from it is instantaneous, i.e. very fast that keeps it empty.

**Second rate equation**

The second rate equation has been written in the Risk's paper as follows:

$$\frac{d\Phi}{dt} = \frac{c\sigma}{n}\iiint \Delta N(r,z)\Phi\phi_0(r,z)dV - \frac{\Phi}{\tau_q} = 0. \quad (2.24)$$

In equation 2.24 the term $\frac{d\Phi}{dt}$ represents the rate of change in the total number of photons in the cavity.

Let's compare equation 2.17 with equation 2.24. The term $\frac{c\sigma}{n}\iiint \Delta N(r,z)\Phi\phi_0(r,z)dV$ represents the total number of photons generated inside the gain medium through stimulated emission.

As before, the term $-\frac{\Phi}{\tau_q}$ stands for the rate with which photons disappear in the cavity due to the presence of losses. These losses are introduced either by the output coupler or the internal cavity loss. $\tau_q$ is called the cold cavity photon life time and it can be found from $\tau_q = \frac{2nl}{c(T+L_i)}$ expression, where T is the loss introduced by the transmission of the output coupler and $L_i$ is the internal cavity loss introduced due to the imperfections of the optical elements.

**Population inversion**

The first rate equations 2.19 and 2.20 represent populations of electrons in the levels $N_2$ and N1, respectively. Considering a two level system, the population inversion (with respect to time) can be found by subtracting the population of the level $N_1$ (lower level) from the population of the level $N_2$ (upper level). Therefore,

$$\frac{\Delta N(r,z)}{dt} = (f_1 + f_2)Rr_p(r,z) - \frac{\Delta N(r,z) - \Delta N^0}{\tau} - \frac{(f_1+f_2)c\sigma\Delta N(r,z)}{n}\Phi\phi_0(r,z) = 0. \quad (2.25)$$

Equation 2.25 represents a spatial distribution of the population inversion with respect to time. Similar to the previous discussion, the terms on the right hand side of equation 2.25 represent the

rates of change in population generated through the pump (i.e. the term $(f_1 + f_2)Rr_p(r,z)$ ), spontaneous emission (i.e. the term $-\frac{\Delta N(r,z)-\Delta N^0}{\tau}$) and stimulated emission (i.e. the term $-\frac{(f_1+f_2)c\sigma\Delta N(r,z)}{n}\Phi\phi_0(r,z)$).

It is worth mentioning that in the thermal equilibrium the unpumped (i.e. initial) population of the level $N_1$ is much larger than that of level $N_2$ (i.e.$N_1^0 \gg N_2^0$). This means that equation 2.18 can be re-written as $\Delta N^0 \cong N_1^0$.

**Population inversion with respect to threshold**

In this part the rate equations are considered for two cases in which the laser either is working bellow threshold or at threshold and above it.

Bellow threshold, we don't have laser photons Φ. The first rate equation can then be used for this condition. As we saw before, the population inversion equation resulted from the first rate equation. Equation 2.25 for the population inversion in thermal equilibrium ($\Phi = 0$) can be written as follows:

$$\Delta N(r,z) = \tau(f_1 + f_2)Rr_p(r,z) - N_1^0. \qquad (2.26)$$

In equation 2.26, if there wasn't unpumped population in the level $N_1$ (i.e. $N_1^0 \cong 0$), the spatial distribution of the population inversion would be same as the pump's spatial distribution. Having such unpumped population, the spatial distribution of the population inversion decreases uniformly in the gain medium.

Let's consider the first rate equation for the threshold and above the threshold. In thermal equilibrium $N_1^0 \gg N_2^0$ and we can say that $N_2^0 \cong 0$. Therefore equation 2.25 can be written as follows:

$$f_f R r_p(r,z) = \frac{\Delta N(r,z) - N_1^0}{\tau} + \frac{f_f c\sigma \Delta N(r,z)}{n} \Phi \phi_0(r,z). \tag{2.27}$$

where $f_f = f_1 + f_2$. Multiplying both sides by $\tau$ yields:

$$\tau f_f R r_p(r,z) = \Delta N(r,z) - N_1^0 + \frac{\tau f_f c\sigma \Delta N(r,z)}{n} \Phi \phi_0(r,z). \tag{2.28}$$

Therefore, the spatially dependent population inversion at threshold and above the threshold can be written as following:

$$\Delta N(r,z) = \frac{\tau f_f R r_p(r,z) + N_1^0}{1 + \frac{\tau f_f c\sigma}{n} \Phi \phi_0(r,z)}. \tag{2.29}$$

Since the second rate equation is dealing with the rate of change in the total number of laser photons, it could only be considered at threshold or above the threshold. Let's rewrite equation 2.24 as follows:

$$\frac{c\sigma}{n} \iiint \Delta N(r,z) \Phi \phi_0(r,z) dV = \frac{\Phi}{\tau_q}. \tag{2.30}$$

Simplifying equation 2.30 yields:

$$\iiint \Delta N(r,z) \phi_0(r,z) dV = \frac{n}{\tau_q c\sigma}. \tag{2.31}$$

In equation 2.31 the spatial distribution of the population inversion in the laser mode area (i.e. left hand side of the equation) is equal to a threshold value from equation 2.29.

**Ratio of a pump beam waist to a laser beam waist**

Let's define $a$ as a ratio of a pump beam waist $w_p$ to a laser beam waist $w_L$.

Equation 2.29 shows that below gain saturation level the spatial distribution of population inversion $\Delta N(r,z)$ can change as a function of the pump distribution $r_p(r,z)$ and the laser distribution $\phi_0(r,z)$.

If $a$ is much smaller than 1 the gain medium will be saturated approximately uniformly. [See figure 2 a and b in the Ref.6]. If $a$ is larger than 1, the gain medium will be saturated mainly in the middle. However there are unsaturated regions around the center of the gain medium. [See figure 2c in the Ref.6]

In addition, the term $\iiint \Delta N(r,z)dV$ in the equation 2.31 shows the variation of population inversion inside the gain medium. This means that the total population inversion (or gain) above the threshold depends on a [6].

In the equation 2.31 if $a \to 0$, the term $\phi_0(r,z)$ will be approximately constant over the spatial distribution of population inversion. Therefore, according to the equation 2.31, the total population inversion stays at the threshold value [6].

In the equation 2.31 if $a \to \infty$, the laser spatial distribution will saturate the gain medium only in a small area. Outside of that area in the gain medium there would be unsaturated parts. This means that by increasing the pump the gain will increase [6].

In the equation 2.31 if $0 < a < \infty$ (i.e. $a$ has intermediate value) the gain highly depends on pump. By increasing the pump power above the threshold the population inversion starts to

increase from its threshold value to the point that the pump saturates the gain medium even far away from its center [6].

It is worth mentioning that, as can be seen from equation 2.29, the spatially dependent population inversion $\Delta N(r,z)$ is a function of the laser intensity and it also depends on population in the lower laser level. This explains the reabsorption loss phenomena introduced by having a thermally populated lower laser level [6].

**Threshold and the *f* function**

The final goal is to find a relationship between the pump and internal laser power. Having internal laser power as a function of the pump power, will lead us to a relationship between the pump power and the laser output power. One way is to consider the results obtained from both rate equations together. In order to do that the population inversion from equation 2.29 can be substituted into equation 2.31. By solving this, the relationship can be found. However, Risk's paper proceeds with another method which covers different approaches to longitudinally pumped CW laser modeling [6].

The gain of a laser as a function of space can be found as follows:

$$G(r,z) = \sigma N(r,z). \tag{2.32}$$

Substituting equation 2.29 into 2.32 yields:

$$G(r,z) = \frac{\sigma\tau f R r_p(r,z)}{1+\frac{\tau f c\sigma}{n}\Phi\phi_0(r,z)} - \frac{\sigma N_1^0}{1+\frac{\tau f c\sigma}{n}\Phi\phi_0(r,z)}. \tag{2.33}$$

In equation 2.33, the term $\frac{\sigma\tau f R r_p(r,z)}{1+\frac{\tau f c\sigma}{n}\Phi\phi_0(r,z)}$ represents a saturable gain and the term $\frac{\sigma N_1^0}{1+\frac{\tau f c\sigma}{n}\Phi\phi_0(r,z)}$ represents a saturable loss introduced by reabsorption loss caused by the thermally populated lower laser level. As can be seen, the first term depends on the pump's spatial distribution and laser's spatial distribution while the second term only depends on the laser's spatial distribution. It is worth mentioning that taking into account the reabsorption loss is an advantage of the Risk's model.

One-way laser intensity per one round trip can be defined by the following equation:

$$I(r,z) = \left(\frac{ch\nu_L}{2n}\right)\Phi\phi_0(r,z). \tag{2.34}$$

Multiplication of the laser gain function by its one-way intensity function results in variation of the one-way laser intensity inside the gain medium with respect to laser axis:

$$\frac{dI(r,z)}{dz} = G(r,z)I(r,z). \tag{2.35}$$

Writing equation 2.35 for the unsaturated gain[2] yields:

$$\frac{dI(r,z)}{dz} = \frac{G^0(r,z)I(r,z)}{1+2sI(r,z)}. \tag{2.36}$$

In equation 2.36, the factor of 2 represents two passes of the one-way laser intensity and s is the saturation parameter $s = \frac{f\sigma\tau}{h\nu_L}$.

[2] Writing the first rate equation in steady-state conditions for both upper and lower level in a general laser system and considering the population inversion relation (i.e. $N = N_2 - N_1$), the relation between the gain and the population (i.e. $G = \sigma N$), and by doing mathematical simplification equation 2.36 can be found .

It is worth mentioning that the steady-state conditions for rate equations is a condition in which there is an equal number of upward (pump excitation) and downward (cased by stimulated and spontaneous emission) transitions [9](i.e. ($\frac{dN_1(r,z)}{dt} = \frac{dN_2(r,z)}{dt} = 0$)[3] )

Comparing equation 2.36 with equation 2.33 yields:

$$G^0(r,z) = \sigma\tau f R r_p(r,z) - \sigma N_1^0. \tag{2.37}$$

Considering a condition when the gain balances the loss yields:

$$\int_{round\ trip} dP_L(z) = 2\int_0^l \frac{dP_L(z)}{dz}dz = P_L(L_i + T). \tag{2.38}$$

where $P_L$ is the average laser power inside the cavity which approximately stays the same under the condition that we have a small loss. $P_L(z)$ is the power in the location z along the laser axis and can be found as follows:

$$P_L(z) = 2\pi\int_0^\infty I(r,z)rdr. \tag{2.39}$$

Substituting equation 2.39 into 2.38 yields:

$$4\pi\int_0^l \frac{d\int_0^\infty I(r,z)rdr}{dz}dz = P_L(L_i + T). \tag{2.40}$$

Substituting equation 2.36 into 2.40 yields:

$$4\pi\int_0^l\int_0^\infty \frac{G^0(r,z)I(r,z)}{1+2sI(r,z)}rdrdz = P_L(L_i + T). \tag{2.41}$$

In equation 2.38, losses (i.e. $L_i$ and T) are considered to be small. In case that we have larger values for the loss (for instance if the output coupler's transmission larger than 15 % was used) the loss should be replaced by logarithmic losses. Therefore, for large output couplers expression $-\ln(1-T)$ should be used [11].

In the Risk's paper, the following parameters were defined:

$$x = \frac{2r^2}{w_p^2}, \tag{2.42}$$

$$B = \frac{2N_0^1 \sigma l}{L_i + T}, \tag{2.43}$$

$$F = \frac{4P_p \tau \sigma \eta_a}{\pi h \nu_p w_L^2 (L_i + T)}, \tag{2.44}$$

$$S = \frac{2c\sigma\tau\Phi}{n\pi w_L^2 l}, \tag{2.45}$$

where, F and S are normalized parameters which are proportional to the pump power and the intracavity laser power, respectively.

Re-writing equation 2.41 based on the above parameters and equations 2.34, 2.37 yields:

$$f_f F \int_0^\infty \frac{\left[\exp(-x) - \frac{Ba^2}{f_f F}\right] \exp(-a^2 x)}{1 + f_f S exp(-a^2)} dx = 1. \tag{2.46}$$

Solving equation 2.46 for F yields:

$$F = \frac{1 + \frac{B}{f_f S} Ln(1 + f_f S)}{f_f \int_0^\infty \frac{\exp[-(a^2+1)x]}{1 + f_f S\, exp(-a^2 x)} dx}. \tag{2.47}$$

When intracavity laser power is close to zero, the laser is working around the threshold. Therefore, solving equation 2.47 to find F for S=0 results in the following equality:

$$F_{th} = \frac{(1 + a^2)(1 + B)}{f_f}. \tag{2.48}$$

Substituting $a = \frac{w_p}{w_l}$ and equations 2.43 and 2.44 into equation 2.48, results in

$$\frac{4P_p\tau\sigma\eta_a}{\pi h\nu_p w_L^2(L+T)} = \frac{\left(1+(\frac{w_p}{w_l})^2\right)\left(1+\frac{2N_0^1\sigma l}{L_i+T}\right)}{f_f}. \tag{2.49}$$

Equation 2.49 holds for the threshold pump power therefore the incident threshold pump power is:

$$P_{\text{th}} = \frac{\pi h\nu_p\left(w_L^2+w_p^2\right)\left(L_i+T+2N_1^0\sigma l\right)}{4\sigma\tau\,\eta_a f_f}. \tag{2.50}$$

The next step is to find variation of the intracavity laser power with respect to the pump power. Since F and S are normalized parameters which are proportional to the pump power and intracavity power, respectively, derivative of S with respect to F results in an expression for variation of the intracavity laser power with respect to the pump power.

Therefore, taking derivative of equation 2.47 with respect to S yields:

$$\frac{dS}{dF} = \frac{1+\frac{B}{f_f S}\ln\left(1+f_f S\right)}{{f_f}^2F^2\int_0^\infty \frac{\left[\exp(-x)-\frac{Ba^2}{f_f F}\right]\exp(-2a^2x)}{\left[1+f_f S\exp(-a^2x)\right]^2}dx}. \tag{2.51}$$

As can be seen in equation 2.51, dS/dF can be found numerically for different ratios of $F/F_{th}$ and fixed values of B, $a$ and $f_f$. On the other hand, $F/F_{th}$ is the same as the ratio of the pump power to the threshold power. Therefore we can define an $f$ function as a special solution of dS/dF when equation 2.51 is numerically solved for different ratios of the pump power to the threshold power for fixed values of B , $a$ and $f_f$.

## 2.4 Output power and efficiencies

In this section, an equation corresponding to the output power of a CW laser is introduced. Based on this equation, the slope and optical to optical efficiencies will be defined.

Equation 2.52 represents the output power of a laser in a continuous wave regime [11, 6]:

$$P_{out} = \frac{-\ln(1-T)}{-\ln(1-T)+L_i} \times \frac{\nu_L}{\nu_P} \times \eta_a \times f\left(\frac{P_{\mathrm{p},inc}}{P_{\mathrm{th}}}\right) \times \left(P_{p,inc} - P_{\mathrm{th}}\right). \tag{2.52}$$

The $f$ function shows a change in the ratio of the intracavity power to the pump power as a function of the incident pump power $P_{p,inc}$ divided by the threshold pump power $P_{th}$. This function is denoted as dS/dF in the W. Risk's paper.

By simplifying equation 2.52 for small output coupler values, we have a familiar expression of the output power:

$$P_{out} \cong \frac{T}{T+L_i} \times \frac{\nu_L}{\nu_P} \times \eta_a \times f\left(\frac{P_{\mathrm{p},inc}}{P_{\mathrm{th}}}\right) \times \left(P_{p,inc} - P_{\mathrm{th}}\right). \tag{2.53}$$

By multiplying the absorption efficiency $\eta_a$ to the incident pump power and threshold power, equation 2.48 can be re-written for the absorbed pump power as follows:

$$P_{out} \cong \frac{T}{T+L_i} \times \frac{\nu_L}{\nu_P} \times f\left(\frac{P_{\mathrm{p},inc}}{P_{\mathrm{th}}}\right) \times \left(P_{p,abs} - P_{\mathrm{th,abs}}\right). \tag{2.54}$$

Considering equation 2.52, we have the following expression for the slope efficiency $\eta$:

$$\eta = \frac{-\ln(1-T)}{-\ln(1-T)+L_i} \times \frac{\nu_L}{\nu_P} \times \eta_a \times f\left(\frac{P_{\mathrm{p},inc}}{P_{\mathrm{th}}}\right). \tag{2.55}$$

Figure 6 shows a simple schematic of an ideal CW laser output versus input pump power graph. As can be seen from equation 2.55 the slope efficiency is not a linear function. However, in a

practical situation especially well above the threshold the slope efficiency is very close to a linear function. This will be discussed further in Chap.3.

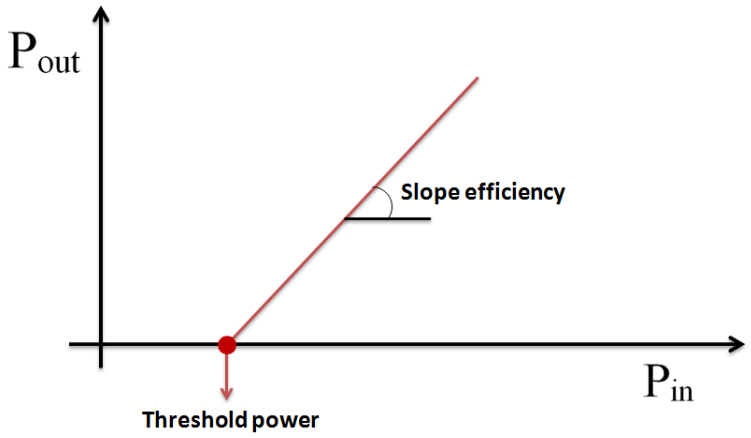


Figure 2.6 Simple schematic of an ideal CW laser output versus input pump power graph

To find out how much of laser output power will be generated by providing a certain amount of optical pump power, another parameter, called optical to optical efficiency, can be defined. This efficiency is the ratio of the output power to the pump power. Therefore, the optical to optical efficiency is

$$\eta_{op-op} = \frac{P_{out}}{P_{\mathrm{p},inc}}. \tag{2.56}$$

## 2.5 Internal cavity loss (Findlay-Clay method)

As we saw in section 2.3, there are two losses in a laser cavity: the loss introduced by an output coupler (T) which extracts the internal cavity power and the internal cavity loss ($L_i$) cased by the imperfections of the optical elements. This section is devoted to an experimental method called Findlay-Clay method [12]. This method can be used to find internal cavity loss in a laser cavity.

Since internal cavity loss (or resonator loss) is caused by imperfection of various optical elements it is always considered as an undesired loss. Finding internal cavity loss is helpful for optimization of laser efficiency [9].

Consider a two mirror laser cavity (optical resonator) and a condition that we have a photon density due to the amplification of a gain medium (optical amplifier) [9]. The photon density after a round trip will see two losses introduced by the two mirrors. Still some part of that energy will be reflected back by the first and second mirrors denoted as $R_1$ and $R_2$ respectively. In the real cavities, $R_1$ is related to reflection of all mirrors in the cavity at the working wavelength (except for an output coupler) and $R_2$ stands for the reflection of the output coupler. Therefore, in general we have losses introduced by the optical resonator and a gain introduced by the gain medium.

Laser threshold is a condition in which the gain balances the loss [9]. Mathematical expression of this condition is as follows [9].

$$R_1 R_2 \exp 2(g - \alpha) l = 1, \tag{2.57}$$

Where g is the gain of the optical amplifier at threshold, l is the length of the gain medium, and $\alpha$ is an effective loss introduced by scattering, absorption or reflections from all cavity elements. This loss is called distributed or effective absorption coefficient which is proportional to the length of the gain medium or laser cavity [9]. Since a round trip is considered (there are two passes of the gain medium) there is a factor of 2 in the above equation.

Therefore, the gain at threshold can be found from the above equation as follows:

$$g = \frac{1}{2L}\ln\frac{1}{R_1R_2} + \alpha. \tag{2.58}$$

The gain of a laser has a relation with the population inversion and emission cross section $\sigma$. Considering the gain at threshold, equation 2.32 can be written as follows: [12]

$$g = \sigma N_t, \tag{2.59}$$

where $N_t$ is the population inversion generated between the upper laser level and the lower laser level at threshold. Considering equations 2.58 and 2.59 together, the population at threshold can be found as follows:

$$N_t = \frac{1}{\sigma}\left[\frac{1}{2L}\ln\frac{1}{R_1R_2} + \alpha\right]. \tag{2.60}$$

Equation 2.61 is a relation between the pump energy at threshold ($E_t$) and $N_t$ introduced in the Findlay and Clay article [12].

$$N_t = AE_t, \tag{2.61}$$

where A is a constant which is proportional to a duration of excitation pulse. Substituting equation 2.60 into equation 2.61 yields:

$$E_t = \frac{1}{\sigma A}\left[\frac{1}{2L}\ln\frac{1}{R_1R_2} + \alpha\right]. \tag{2.62}$$

We can proceed to the final equation by defining $E_{t0} = \frac{\alpha}{A\sigma}$ which is the energy at threshold for a zero output coupler. Therefore [12]:

$$E_t = E_{t0}[\frac{1}{2\alpha L}\ln\frac{1}{R_1R_2} + 1]. \tag{2.63}$$

$R_2$ is the reflection of an output coupler and T is the transmission of an output coupler, therefore $R_2$ = 1-T. $R_1$ is the reflection of the other mirror. In a laser cavity transmission (or loss) of the internal cavity power is expected only by its output coupler. However, there would be some loss introduced by the other optical elements. Therefore, $R_1 = 1 - \delta$ where δ is a logarithmic internal cavity loss. Since loss inside the cavity and loss due to the transmission of output coupler are small, the above equation can be simplified as follows

$$E_t = E_{t0}[\frac{1}{2\alpha L}(L_i + T) + 1], \tag{2.64}$$

where $L_i$ is the internal cavity loss.

Considering equation 2.64, it can be seen that by changing the output coupler and measuring the corresponding threshold energy, a value for the internal cavity loss can be found from this linear relationship. This is the main idea of the Findlay-Clay analysis.

As we can see in the Findlay and Clay article [12], a relation between the threshold energy, output coupler and internal cavity loss had been established. This relation is useful for finding internal cavity loss in a laser pumped by a lamp working in pulsed regime. However, nowadays longitudinal pumping by laser diodes is very popular. To find internal cavity loss in these lasers a relation between the threshold pump power, output coupler and internal cavity loss should be used.

In section 2.3.2, a relation was found for internal cavity power. According to it when the internal cavity power is zero (S=0), we are working around the threshold. Therefore, an equation for threshold pump power was introduced (equation 2.50). When $N_1^0 \cong 0$ (a case of 4-level lasers) this equation can be re-written as follows

$$P_{\text{th}} = \eta_F \, (L_i + T), \tag{2.65}$$

where $\eta_F = \frac{\pi h \nu_p (w_L^2 + w_p^2)}{4\sigma\tau \, \eta_a}$ . Therefore, by changing the output coupler and measuring the corresponding threshold pump power and fitting the data to the equation 2.65, a value for the internal cavity loss can be found. To be more accurate, T can be replaced by a logarithmic expression of loss due to the transmission of the output coupler (e.g. $\ln \frac{1}{R_1} = -\ln(1-T)$ ). This yields

$$P_{\text{th}} = \eta_F \, (L_i - \ln(1-T)). \tag{2.66}$$

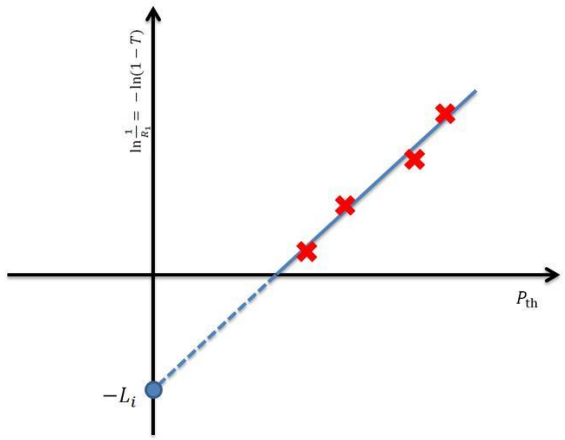


Figure 2.7 Findlay Clay method for a 4 level laser longitudinally pumped by a laser diode

Figure 2.7 schematically shows Findlay-Clay method for finding internal cavity loss of a 4 level laser longitudinally pumped by a laser diode. In this figure the red signs are the measured threshold powers for different output couplers. The blue line is a linear fit for the equation 2.66. As can be seen, the point where the blue line crosses the vertical axis corresponds to the internal cavity loss value.

## 2.6 VCSEL

In this section the vertical cavity surface-emitting lasers (VCSELs) are briefly introduced. In the next chapter VCSEL's parameters will be used to numerically explore its applicability as a pump source.

In 1979 Professor Kenichi Iga started research on a new laser device called VCSEL and in 1979 first article [13] on VCSEL was published [14]. In 1988 Professor Iga reported room temperature operation of VCSEL and after that other groups started research on VCSEL [15]. Nowadays, the production of VCSELs has become the second largest among the semiconductor laser industry [14]. Edge emitting laser diodes are replaced by VCSELs in optical disk drives and also in multimode fiber based optical communication for Giga bit per second data transmission [14] and it is continuing to show its advantages over the edge emitting laser diodes.

### 2.6.1 Device geometry

VCSELs have two main parts: active region and two distributed brag reflectors (DBR). Figure 2.8 shows the basic schematic of VCSELs and edge emitting lasers. As can be seen, in VCSELs there are bottom and top mirrors which are DBRs and also a region called active region. The structure of edge emitting lasers can also be divided into the same two main parts. It is worth mentioning that in edge emitting lasers the cleaved surface of a facet acts as a mirror.

Active region is consisting of one or more quantum wells. The thickness of the active region affects the threshold current density. To have reasonable threshold current density the active region should be small enough [16]. Therefore, with a thinner active region a lower threshold current is achievable. Likewise, with a thicker active region a higher output power can be reached [14]. Moreover, the diameter of the whole device will affect the threshold current [16]. The smaller the diameter of the device is, the lower the threshold current will be. In addition,

having a small diameter (on the order of few microns) will result in having a single transverse mode [14].

Having a thin active region, means that the gain path in the laser cavity is small (around 1%). Therefore, a high reflectivity (more than 99%) of the DBRs is very critical to maintain laser operation [16 and 17].

DBRs are made by putting consequent layers with low and high refractive indices on top of each other and the thickness of DBRs are λ/4 where λ is the laser wavelength [14]. Each layers of DBR partially reflects the incident light and finally these reflections will be added constructively. This means that having a higher number of layers results in higher reflectivity of DBR. Typically more than 20 pairs of layers are required. [14]

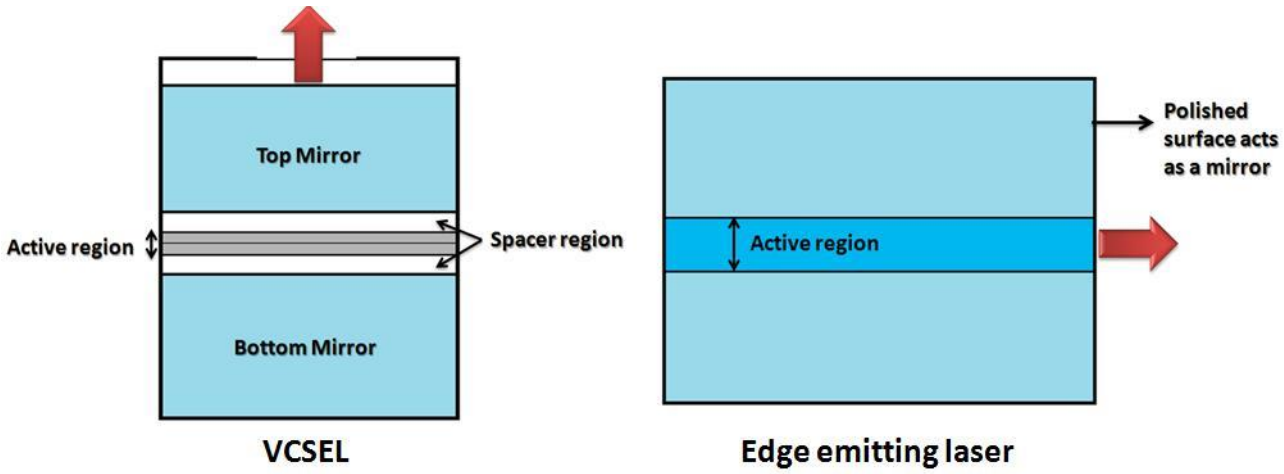


Figure 2.8 Basic schematic of VCSELs and edge emitting lasers

It is worth mentioning that the fabrication process of VCSEL is done by the Molecular beam epitaxy (MBE) or Metal–organic chemical vapor deposition (MOCVD) with precise growth rate [17].

### 2.6.2 Features

In fabrication process of the traditional edge emitting laser diodes one step is dicing. Having this step means integration of this device with the other optoelectronics is hard and also manufacturing process is relatively expensive compared to that one of VCSELs [15].

In comparison with edge emitting laser diodes, penetration of the optical field into the multilayer structure and also having a small gain path (i.e. small active region) affects the threshold and output of VCSELs [14]. In VCSELs the active region can be fabricated to be short and consequently the losses introduced by the cavity should be very small. Having short cavity with low amount of loss makes threshold of VCSEL small compared to the edge emitting laser diodes [18]. It is worth mentioning that having a short cavity will results in oscillation of one longitudinal mode inside the VCSEL [19].

Due to the geometry of VCSEL structure, its beam shape will be circular. Therefore, unlike edge emitting laser diodes we can have equal $M^2$ in both vertical and horizontal directions.

The wavelength shift due to the temperature variations in VCSELs happens as a result of changes in the geometrical size of the cavity and also in the effective refractive index [14]. This means that the thermal shift of the wavelength depends on the properties of the materials used in the fabrication of VCSELs [14].

## 2.7 Conclusion

This chapter can be divided into the three main parts: modeling of a 4 level CW laser with longitudinal pumping, internal cavity losses and overview of the VCSEL.

This chapter started with the Helmholtz equation and its solution which was a Gaussian beam. Considering a CW laser pumped by a pump with Gaussian distribution and using the Risk model,

parameters defined by the rate equations were connected to the longitudinal pumped laser. The final results of the Risk model were equations for the output power and the threshold pump power of a longitudinally pumped CW laser. It is worth mentioning that the output power equation is related to the $f$ function. This function depends on ratios of the pump power to the threshold power for fixed values of B , $a$ and $f_f$. The equations that the $f$ function can be found from were obtained for a condition that the laser and pump beams were assumed to have a Gaussian intensity distribution.

An important parameter in the model is the internal cavity loss. An experimental method called Findlay-Clay method for finding this parameter was explained.

The final part of this chapter was devoted to a device called VCSEL. Basic parts of the device and some of its features were briefly discussed.

# Chapter 3

# Design of a longitudinally pumped continuous wave laser

## 3.1. Introduction and motivation

In chapter 2, the Risk model was explained in detail. In this chapter, this model will be used for modeling of a CW Nd:$YVO_4$ and Nd:YAG lasers longitudinally pumped by high power VCSEL modules at 808 nm. Having known properties of the pump and the gain medium, the presented method in this work can be used to design an optimized CW laser.

Recent progress in high power vertical-cavity surface-emitting lasers (VCSEL) [20] and their unique features make them a good alternative to the edge emitting laser diodes for longitudinal pumping of solid-state laser gain media. In comparison with edge emitting laser diodes, VCSELs have low threshold current, [14] low fabrication cost, and wavelength stability with temperature variation [21]. The latter feature of VCSELs results in a simplified cooling system of laser pumps as well as increased laser reliability when operating at high temperatures. In addition, having a circular beam shape, VCSELs can become efficient pump sources due to the uniform excitation of a gain medium [22].

On the other hand, among the variety of Nd-ion based gain media, crystals of Nd:$YVO_4$ have relatively high absorption cross section and relatively broad absorption line width at 808 nm [9]. Therefore, narrow emission bandwidth and wavelength stability of VCSELs against changes in temperature make them an attractive optical pump source for longitudinal excitation of Nd:$YVO_4$ lasers at 808 nm.

Previously, VCSEL end-pumped [22] and QCW side-pumped [23] Q-switched Nd:YAG lasers were demonstrated. In this study, commercially available 6 W and 15 W VCSEL modules were studied as the pump sources for a CW Nd:$YVO_4$ laser. To the best of our knowledge, this is the first time that VCSELs were considered and analysed for longitudinal pumping of a CW laser. For each case the optimum output couplers were determined. Next, the calculations of slope efficiency, maximum output power and optical-to-optical efficiency were carried out. In addition, a comparison with pumping of a Nd:YAG crystal has also been presented.

## 3.2. General laser design considerations

This section discusses general laser design guidelines when this process starts with a given pump source. In this case optical characteristics of a pump source such as $M^2$, N.A, emission area and an output power have direct effect on the choice of a gain medium as well as on achievable pump spot size. Both of these factors, i.e. the gain medium (and its refractive index) and the pump spot size, put constraint on the required length of the gain medium through the confocal parameter. Taking these factors into account one can determine the gain medium, the pump spot size and the crystal's length. Figure 3.1 shows a general procedure of designing of a CW laser which starts with characteristics of the pump source.

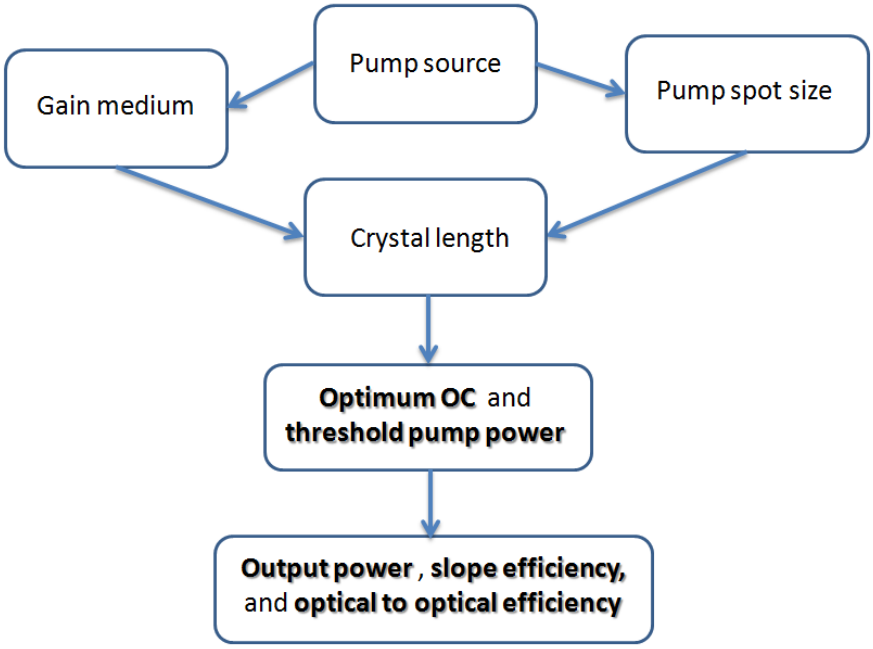


Figure 3.1 A general CW laser design procedure

It is worth mentioning that selecting a longer crystal than that determined by the 10 % confocal parameter can be reasonable when more efficient thermal management is needed. In addition, the pump absorption efficiency of the crystal should be considered for determining the optimized value for the crystal's length.

After selecting the crystal's length, the optimum OC and the required threshold pump power for the selected pump spot size can be found. The output power, slope efficiency and optical to optical efficiency can be determined in the next step. In each step one can return back to the first place and change the pump spot size or the gain medium and its length to reach a specific characteristic of a CW laser.

For example, for a certain pump source, if $A_1$ is selected as an initial spot size then $B_1$ can be selected through the 10% confocal parameter as an initial optimized crystal length for a gain medium $C_1$. Then for this laser system the threshold pump power, optimum OC, output power

and efficiencies can be calculated using the Risk's model for a longitudinally pumped CW laser. Consider a case where it is required to have a design with a lower threshold pump power. Therefore one can return to the first step and change either the pump spot size or the gain medium (or its doping level). For instance, consider a situation when the gain medium cannot be changed. Thus an $A_2$ can be assigned as a newly selected value for the pump spot size and consequently an optimized length of $B_2$ would be selected for the gain medium $C_1$.This process can be repeated several times until a final optimized design will be found for the CW laser.

## 3.3. Model and parameters

In our numerical model, an a-cut Nd:$YVO_4$ (1.1% ) and Nd:YAG (1%) crystals, as two candidates to be pumped by VCSEL modules, were compared. The values used in this work for the crystals parameters are shown in Table 3.1. The value of the absorption coefficient at 808 nm for Nd:$YVO_4$ given by different companies is around 31.2 $cm^{-1}$. However, due to the fact that Nd:$YVO_4$ is naturally birefringent and the output of VCSEL modules is not polarized, half of this value was used in the model. According to Turri, *et al.* work [24] we also have different values for the emission cross section of Nd:$YVO_4$. As a precaution, the lowest value has been selected. The value of the internal cavity loss was set to be 2%.

Table 3.1 Parameters of the a-cut Nd:YVO4 (1.1% ) and Nd:YAG (1%) crystals

| | **Nd:$YVO_4$(a-cut)** | **Nd:YAG** |
|---|---|---|
| **Laser wavelength(nm)** | 1064 | 1064 |
| **Pump wavelength (nm)** | 808 | 808 |
| **Absorption coefficient ($cm^{-1}$)** | 15.6 | 4 |
| **Emission cross section** | $11.5 \times 10^{-19}\ cm^2$[24] (For π polarization) | $2.8 \times 10^{-19}\ cm^2$[9] |
| **Fluorescence lifetime(μs)** | 99 [25] | 230 [9] |
| **Nd doping** | 1.1% | 1% |
| **Refractive index** | 2.165 [26] | 1.82 [9] |
| **Crystal length (mm)** | 1 | 1 |

There are several models for continuous wave operation of lasers [11]. In this work, a space dependent model based on work of W. Risk [6] was considered. Let's consider equation 2.52 in section 2.4:

$$P_{out} = \frac{-\ln(1-T)}{-\ln(1-T)+L_i} \times \frac{\nu_L}{\nu_P} \times \eta_a \times f\left(\frac{P_{\mathrm{p},inc}}{P_{\mathrm{th}}}\right) \times \left(P_{p,inc} - P_{\mathrm{th}}\right). \quad (3.1)$$

This equation represents the output power of a laser in continuous wave regime [6 and11].

As it was explained in chapter 2, the $f$ function shows a change in the ratio of the intracavity power to the pump power as a function of the incident pump power $P_{p,inc}$ divided by the threshold pump power $P_{th}$ [6]. This function is denoted as dS/dF in the W. Risk's paper [6]. The beam distribution of the VCSEL modules is assumed to be a circular Gaussian.

Considering equation 2.50 in Chap.2 and assuming a zero value for the reabsorption loss (i.e. $N_0^1$=0 and B = 0), the threshold pump power of a 4 level laser is given by the equation 3.2. It is worth mentioning that in this equation the $w_p^2$ term was replaced by the $a^2 w_l^2$ term.

$$P_{\mathrm{th}} = \frac{\pi h\, \nu_p \times (1+a^2) \times \left(w_L^2\right) \times (L_i - \ln(1-T))}{4\sigma\tau\eta_a}. \quad (3.2)$$

In order to have a high efficiency, a good overlap between the pump and laser modes is a logical assumption (e.g. $a$=1) for a CW laser. From the experimental viewpoint, by selecting an appropriate length for the crystal we can assume that $a$=1. By substituting this into equation 3.2 we get

$$P_{\mathrm{th}} = \frac{\pi h\, \nu_p w^2 (L_i - \ln(1-T))}{2\sigma\tau\eta_a}, \quad (3.3)$$

where $w$ is the beam waist of the pump and cavity modes inside the crystal .

In a 4 level laser the reabsorption loss is zero (i.e. $N_0^1$=0) and therefore B=0 (see equation 2.43 in section 2.3.2). Considering the above assumptions and a 4 level laser ($f_f = 1$) pumped by a Gaussian beam with $a$=1, the equation 2.51 in section 2.3.2 can be re-written as follows [6]:

$$f\left(\frac{P_{\mathrm{p},inc}}{P_{\mathrm{th}}}\right) = \frac{dS}{dF} = \frac{1}{F^2 \int_0^{\infty} \frac{[\exp(-x)]\exp(-2x)}{[1+S\exp(-x)]^2} dx}. \tag{3.4}$$

As we saw before, equation 2.47 is a relation between the F and S parameters. For a 4 level laser (i.e. $B = 0$ and $f_f = 1$) and $a = 1$ this equation can be rewritten as follows:

$$F = \frac{1}{f \int_0^{\infty} \frac{\exp[-2x]}{1+S\,exp(-x)} dx}. \tag{3.5}$$

The required $f$ function was generated through numerically solving equations 3.4 and 3.5 together (see figure 3.2). As can be seen from figure 3.2, a dramatic change in the function $f$ occurs when $P_{p,inc}/P_{th}$ has relatively small values and the variation of the $f$ function after $P_{p,inc}/P_{th}$ $\cong 10$ is very small.

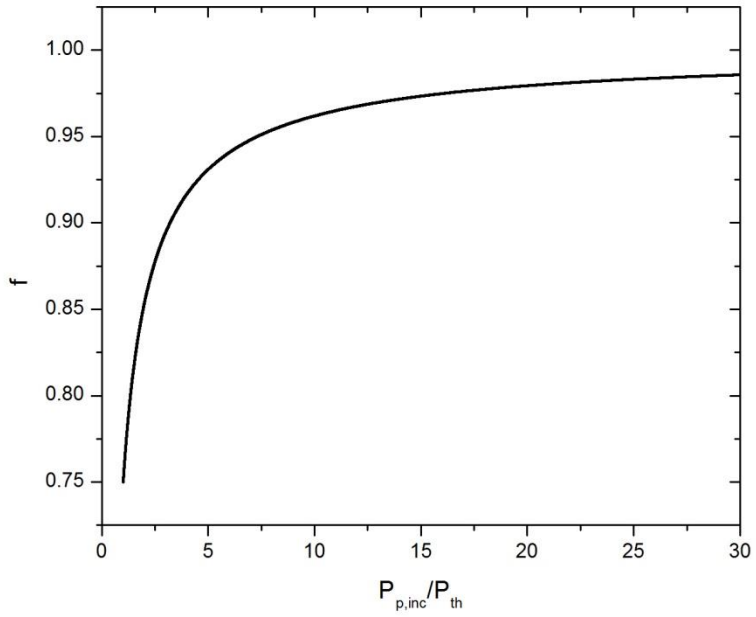


Figure 3.2 Calculation of the *f* as a function of Pp,inc/Pth for a=1 and four level laser.

## 3.4. VCSEL modules

In this work, parameters of two VCSEL modules from Princeton Optronics, shown in Table 3.2, were used. According to the Table 3.2, VCSELs have a small wavelength shift due to the changes in their temperature. Therefore, we assumed that the pump wavelength will stay constant at different output powers. This results in having a constant pump absorption coefficient. The values of the pump and the laser wavelength used in the calculations are mentioned in Table 3.1.

As can be also seen, these VCSEL modules have high beam quality $M^2$ values; this will result in highly divergent pump beams. Considering the beam divergence of these pumps, the 10% depth of focus parameter defined in section 2.2.3 can be used. This parameter is a distance over which the beam waist increases only by 10%. This will ensure that over this length the pump beam

waist will remain almost constant. Therefore, the ratio of the pump beam waist and the laser beam waist will approximately stay the same along the full crystal length. In other words, the 10% depth of focus parameter determines the optimum length for the crystal which will be pumped by a particular VCSEL module. Figures 3.3-3.6 illustrate the 10% depth of focus parameters for 6 W and 15 W VCSEL modules for both Nd:$YVO_4$ and Nd:YAG crystals versus the chosen pump beam radius.

Table 3.2 VCSEL modules data

| VCSEL power (W) | $M^2$ | Threshold current ($\boldsymbol{A}$) | Operating current ($\boldsymbol{A}$) | Maximum Wavelength shift ($\boldsymbol{nm}$/°C) | N.A. | Emission area ($\boldsymbol{mm^2}$) | Beam waist radius ($\boldsymbol{mm}$) | Spectral width (FWHM) ($\boldsymbol{nm}$) |
|---|---|---|---|---|---|---|---|---|
| 15 | 761.27 | 4 | 18 | 0.070 | 0.15 | 2.6×2.6 | 1.3 | 0.8 |
| 6 | 439.19 | 1 | 7 | 0.070 | 0.15 | 1.5×1.5 | 0.75 | 0.8 |

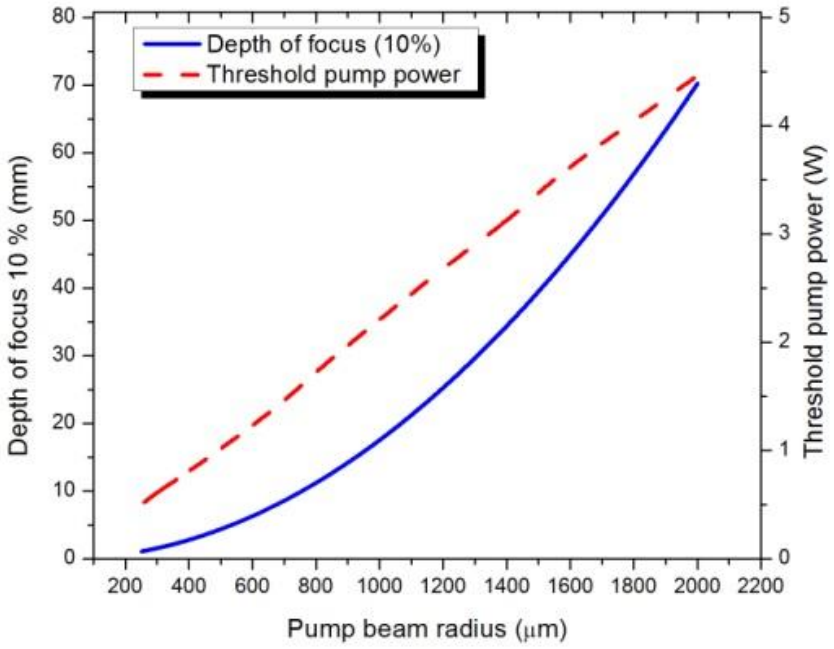


Figure 3.3 Calculation of the 10% depth of focus and the incident threshold pump power for Nd:YVO4 crystal with optimum OC as a function of the beam waist radius for 6 W VCSEL.

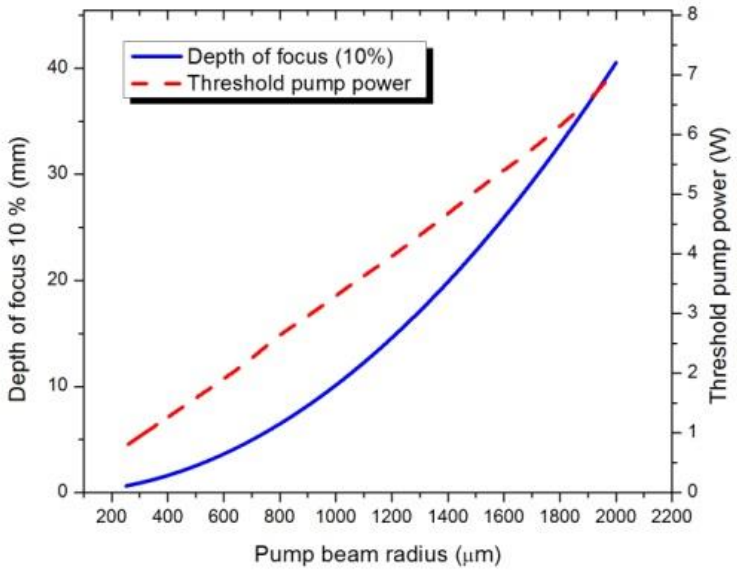


**Figure 3.4 Calculation of the10% depth of focus and the incident threshold power of Nd:YVO4 with optimum OC as a function of the beam waist radius for 15 W VCSEL.**

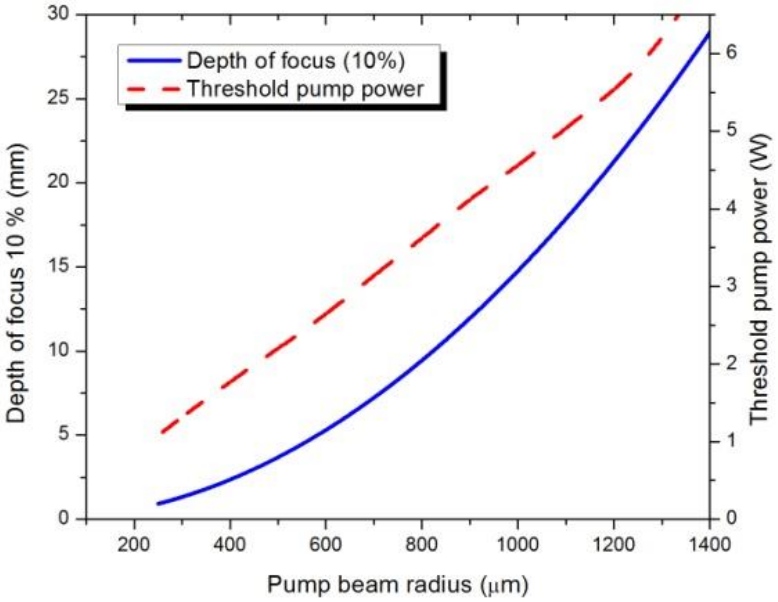


**Figure 3.5 Calculation of the 10% depth of focus and the incident threshold power of Nd:YAG with optimum OC as a function of the beam waist radius for 6W VCSEL.**

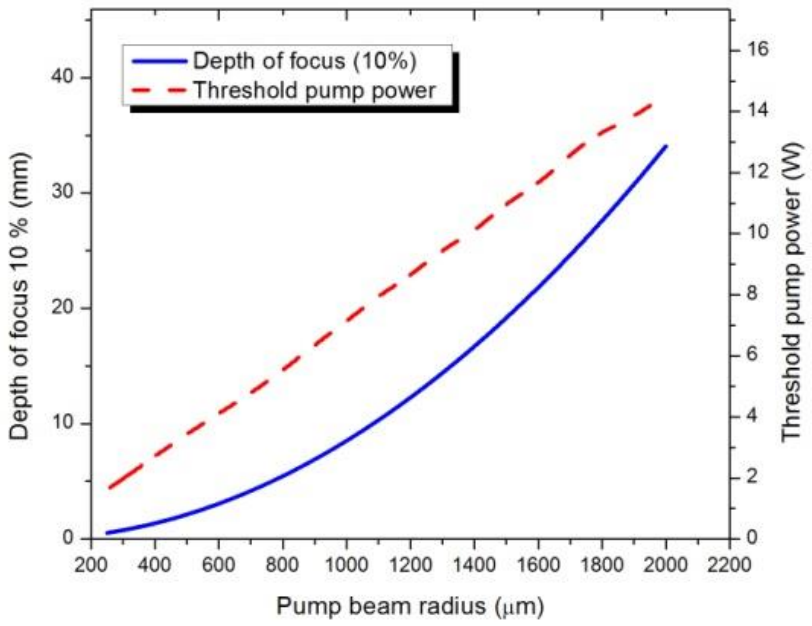


**Figure 3.6 Calculation of the 10% depth of focus and the incident threshold power of Nd:YAG with optimum OC as a function of the beam waist radius for 15W VCSEL.**

By decreasing the pump beam waist, the threshold pump power will decrease and consequently the output power will increase. However, in this case due to the high $M^2$ values, it would be hard to keep the pump beam focused inside the crystal. To be reasonable we assumed that it will be possible to decrease the pump beam waist up to the half of its original size as specified by the manufacturer. Thus, the pump beam waist diameters of 6 W and 15 W VCSEL modules were set to 0.75 mm and 1.3 mm, respectively. Therefore our working points were selected to be at the beam waist radii equal to 0.375 mm and 0.65 mm, respectively. According to the figures 3.3 and 3.4, at these working points the 10% depth of focus parameters will be 2.5 mm and 4.3 mm for 6 W and 15W modules, respectively. This means that if we select a crystal with the length that is shorter than 2.5 mm for 6 W VCSEL and 4.3 mm for 15 W VCSEL, the pump beam waist will stay approximately constant along the whole crystal length. For this work we selected the crystals with the length of 1 mm.

Also shown in figures 3.3-3.6 are plots of the threshold pump powers for the corresponding pump beam radii. The threshold pump power for each pump beam waist radius was calculated using an optimum value of the output coupler *T*. This is the value at which a particular pump spot will result in the highest output power. The values of the optimum output couplers for each pump beam size were calculated in the following way. By substituting the threshold pump power expression from equation 3.3 into equation 3.1, we have:

$$P_{out} = \frac{-\ln(1-T)}{-\ln(1-T)+L_i} \times \frac{\nu_L}{\nu_P} \times \eta_a \times f\left(\frac{P_{\mathrm{p},inc}}{P_{\mathrm{th}}}\right) \times \left(P_{p,inc} - \frac{\pi h\, \nu_p w^2 (L_i - \ln(1-T))}{2\sigma\tau\eta_a}\right). \qquad (3.6)$$

In equation 3.6 considering a fixed pump power value and a specific beam waist, by changing the *T* from 0% to 100% and taking into account dependence of the function *f* on *T* (through $P_{th}$) we can generate a curve which shows the output power as a function of the transmission of the output coupler. In this curve, for a certain output coupler, called the optimum output coupler, we can find the maximum output power for the selected beam waist. An example of this curve for the Nd:$YYO_4$ crystal is shown in figure 3.7 for a fixed pump power of 15 W and a beam waist radius equal to 0.650 mm. As can be seen, for an optimum value of OC around 10% the output power reaches its maximum. This process was repeated for every beam waist and two fixed pump powers. These pump powers corresponded to the nominal power provided by the VCSEL modules, i.e. 6 W and 15 W.

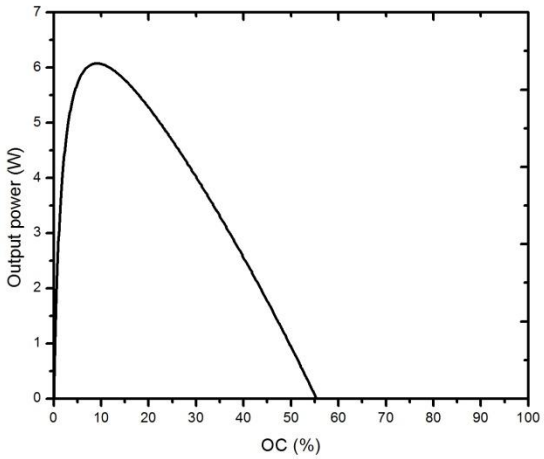


Figure 3.7 Calculated output power from Nd:YYO4 crystal as a function of the OC for a beam waist equal to 0.65 mm and pump power of 15 W.

The threshold pump power was then calculated for various beam waist radii using equation 3.3 and by substituting the calculated values of the optimum output couplers. Figures 3.3 and 3.4 show the results for the Nd:$YVO_4$ crystal pumped by the 6 W and 15 W VCSEL modules, respectively, and figures 3.5 and 3.6 show similar results for the Nd:YAG crystal. At our working points, as illustrated in figures 3.3-3.6, both 6 W and 15 W VCSEL modules have high enough pump powers to work well above the lasing threshold.

In general, figures 3.3-3.6 present our justifications of selecting a particular working point by taking into account the pump parameters such as the beam quality and the available power.

## 3.5. Results and discussions

In previous section, the crystal medium lengths were selected to be 1 mm long and also we showed that both VCSEL modules have enough of pump power to work well above the threshold. In addition, a method to find the optimum output couplers was discussed. Dashed lines in figures 3.8-3.11 show the optimum output couplers for the chosen range of pump beam waist radii for both crystals pumped by 6 W and 15 W VCSELs.

In this section, we will present our results on calculations of maximum achievable output powers, as well as slope and optical-to-optical efficiencies of 1 mm long Nd:YAG and Nd:$YVO_4$ crystals pumped by the considered VCSEL modules. Then, for our selected working points the comparison between both crystals pumped by both VCSEL modules will be presented.

The calculations of the maximum achievable output powers were carried out using equation 3.1 and by substituting the corresponding calculated values of the optimum output couplers and threshold pump powers. Solid lines in figures 3.8-3.11 show the results of these calculations. It is worth mentioning that all assumptions made in section 3.4 were also used in this section and, in particular, the dependence of function $f$ on $T$ was considered. According to these figures, at the selected working points, the maximum output power from the Nd:$YVO_4$ crystal pumped by 6 W and 15 W VCSELs was calculated to be 2.5 W and 6 W, respectively, using a 10 % output coupler. These powers for the Nd:YAG crystal were calculated to be 0.7 W and 1.6 W, respectively, using a 4 % output coupler. Comparing the two crystals, it can be seen that with the same pump beam radius, crystal length and pump power, the maximum achievable output powers from the Nd:$YVO_4$ lasers are more than 3 times higher.

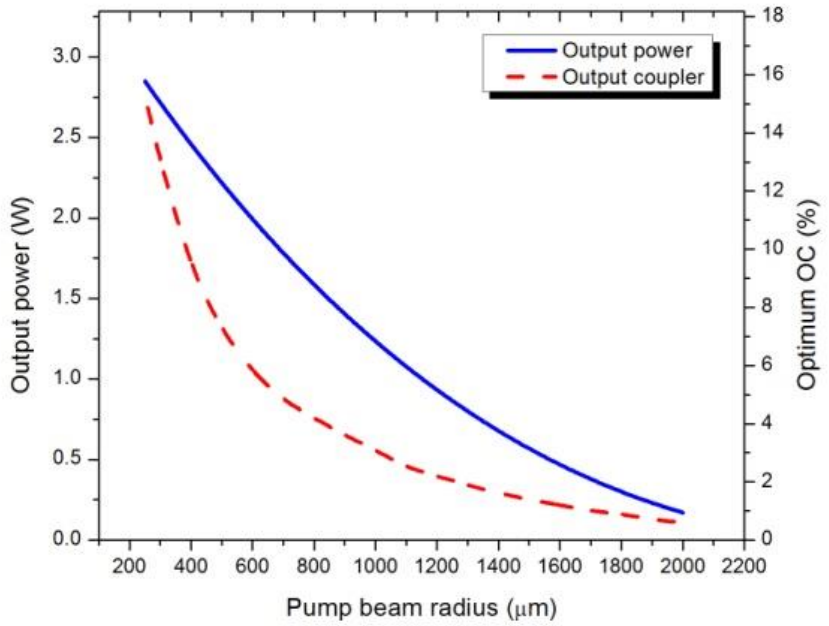


**Figure 3.8 Calculated output power using the optimum OC and the optimum OC as a function of the pump beam radius in Nd:YVO4 crystal pumped by 6 W VCSEL.**

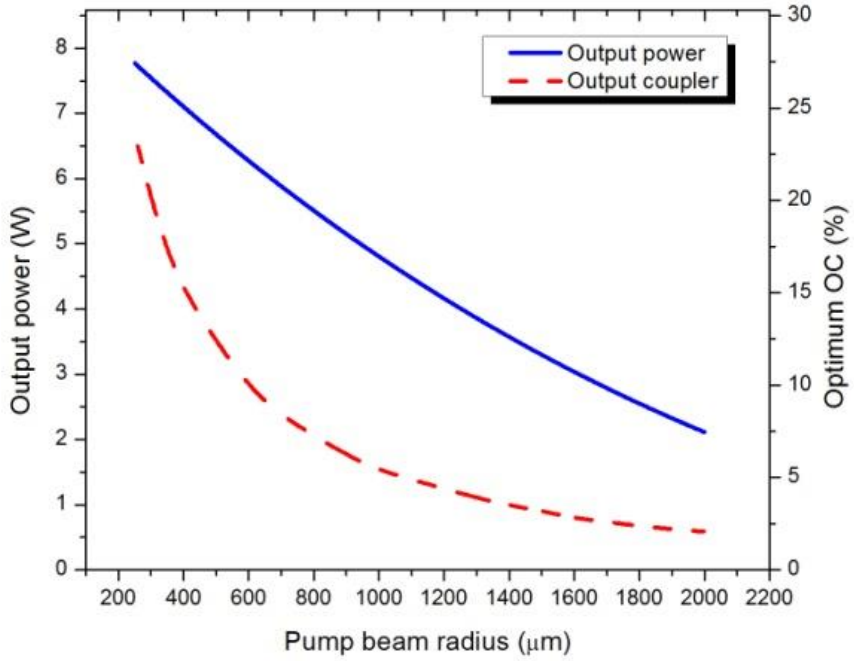


**Figure 3.9 Calculated output power using the optimum OC and the optimum OC as a function of the pump beam radius in Nd:YVO4 crystal pumped by 15W VCSEL.**

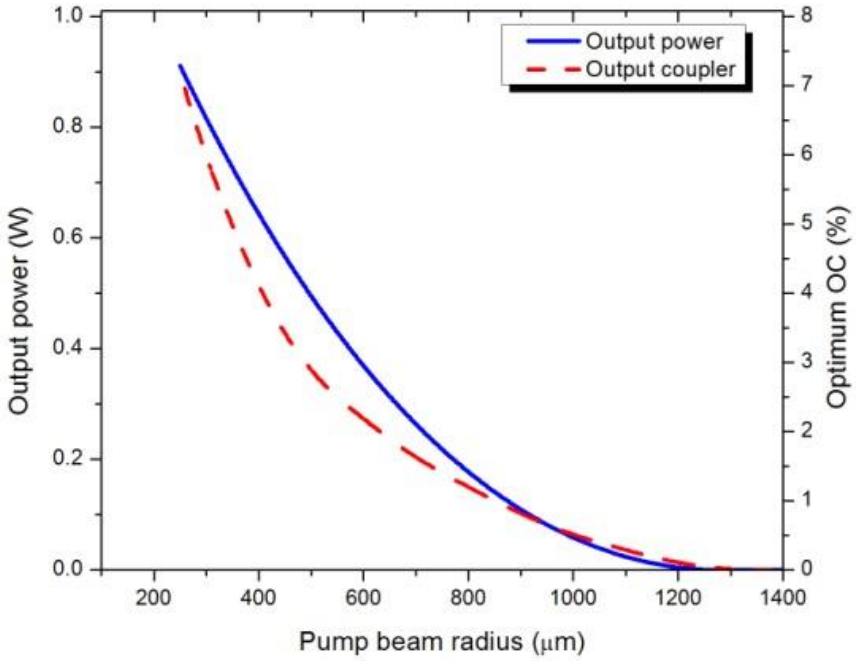


**Figure 3.10 Calculated output power using the optimum OC and the optimum OC as a function of the pump beam radius in Nd:YAG crystal pumped by 6 W VCSEL.**

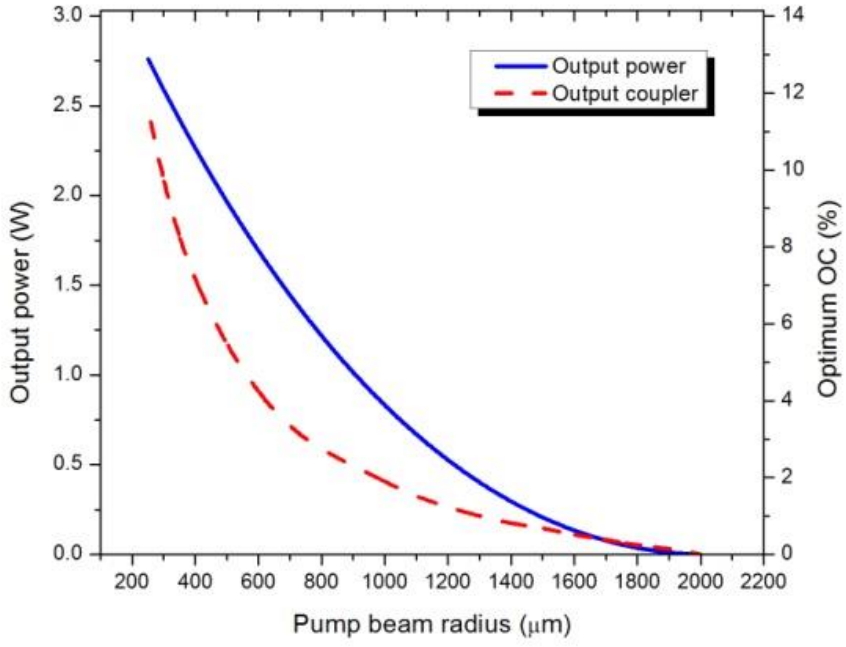


**Figure 3.11 Calculated output power using the optimum OC and the optimum OC as a function of the pump beam radius in Nd:YAG crystal pumped by 15W VCSEL.**

We had the following expression for the slope efficiency $\eta$ in section 2.4:

$$\eta = \frac{-\ln(1-T)}{-\ln(1-T)+L_i} \times \frac{\nu_L}{\nu_P} \times \eta_a \times f\left(\frac{P_{\mathrm{p},inc}}{P_{\mathrm{th}}}\right). \quad (3.7)$$

In equation 3.7, $L_i$, $\nu_L, \nu_P and\ \eta_a$ are constants. Considering the nominal values for the incident pump powers and substituting the calculated values of the corresponding optimum output couplers, threshold powers, and *f* functions into equation 3.7, calculations of the slope efficiency versus the pump beam waists were carried out. In these calculations, the dependence of function *f* on *T* was also considered. Solid lines in figures 3.12-3.15 show the slope efficiency as a function of the pump beam radius in Nd:$YVO_4$ and Nd:YAG crystals. According to these figures, at the selected working points, the slope efficiency for the Nd:$YVO_4$ crystal pumped by 6 W and 15 W VCSELs was calculated to be 48% and 47%, respectively, using the 10% output coupler. These slope efficiencies for the Nd:YAG crystal were calculated to be 16% and 15%, respectively, using the 4% output coupler. Comparing the two crystals it can be seen again that the slope efficiencies of the Nd:$YVO_4$ crystal are about 3 times higher than those of the Nd:YAG crystal.

Optical to optical efficiency is the ratio of the output power to the pump power. This ratio was calculated by dividing the value of each point of the solid lines in figures 3.8-3.11 by their corresponding nominal pump power. Dashed lines in figures 3.12-3.15 show the optical to optical efficiency as a function of the pump beam radius in Nd:$YVO_4$ and Nd:YAG crystals. According to these figures, at the selected working points, the optical to optical efficiency for the Nd:$YVO_4$ crystal pumped by 6 W and 15 W VCSELs was calculated to be 42% and 40%, respectively, using the 10% output coupler. These optical to optical efficiencies for the Nd:YAG

crystal were calculated to be 11% and 10%, respectively, using the 4 % output coupler. As can be seen, optical to optical efficiencies of the Nd:$YVO_4$ crystal with the same pump beam radius, crystal length and pump power are about 4 times larger than those of the Nd:YAG crystal.

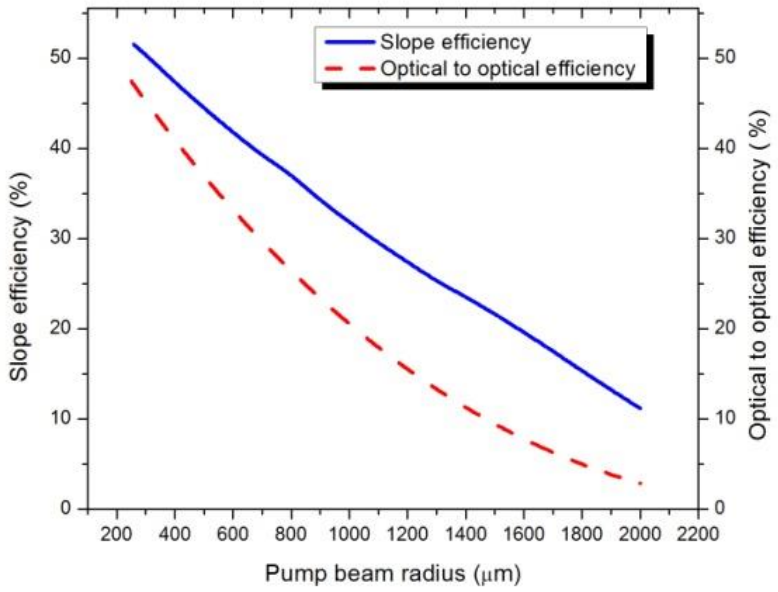


**Figure 3.12 Calculated slope efficiency and optical to optical efficiency as a function of the pump beam radius in Nd:YVO4 crystal pumped by 6 W VCSEL.**

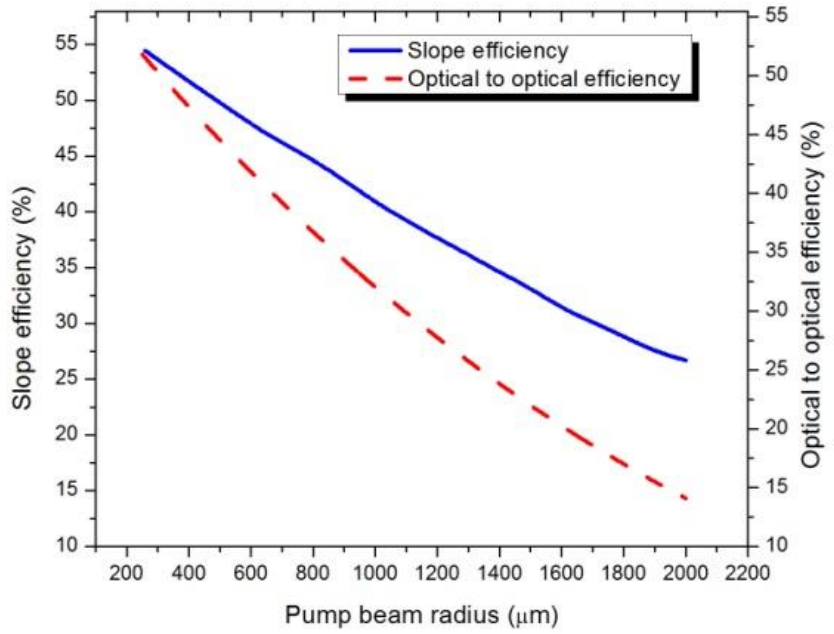


Figure 3.13 Calculated slope efficiency and optical to optical efficiency as a function of the pump beam radius in Nd:YVO4 crystal pumped by 15 W VCSEL.

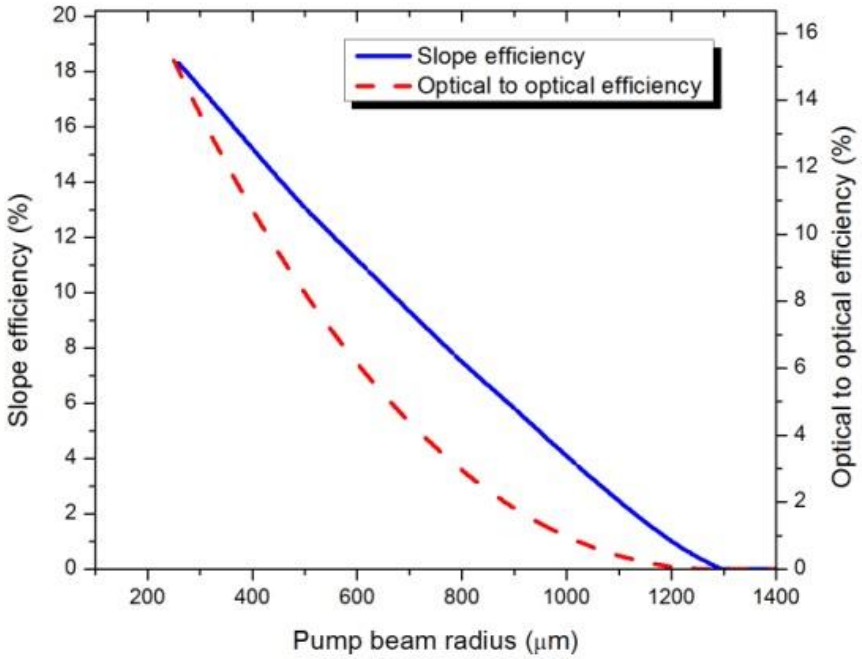


Figure 3.14 Calculated slope efficiency and optical to optical efficiency as a function of the pump beam radius in Nd:YAG crystal pumped by 6 W VCSEL.

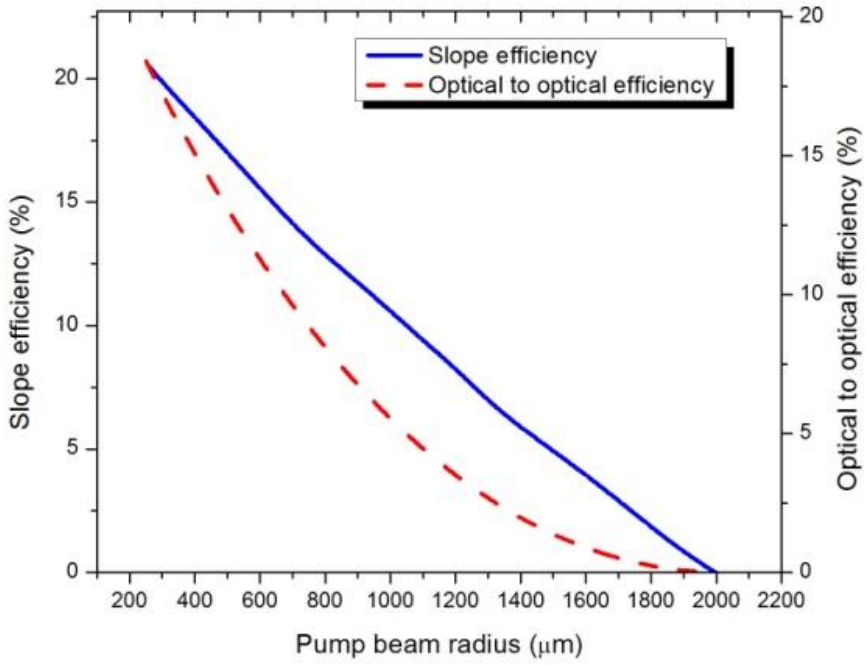


Figure 3.15 Calculated slope efficiency and optical to optical efficiency as a function of the pump beam radius in Nd:YAG crystal pumped by 15 W VCSEL.

In general, as depicted in figures 3.8-3.15, decreasing of the pump beam radius results in higher output power, slope and optical to optical efficiencies. However, the $M^2$ value of the pump beam puts a limit on our ability to decrease the pump beam radius. This shows the importance of the 10% confocal parameter.

Considering equation 3.1 for a fixed pump beam waist and a fixed optimum output coupler, we can generate the output power versus pump power plots for both laser crystals and VCSEL modules. As was discussed in section 3.4, our working points were selected to be at the beam waist radii equal to 0.375 mm and 0.65 mm, for 6 W and 15 W VCSEL modules, respectively. Shown in figures 3.16 and 3.17 are the output powers as a function of the pump power for the both the Nd:$YVO_4$ and Nd:YAG crystals pumped by 6 W and 15 W VCSEL modules. As can be seen from these figures, we can achieve a higher power and a higher slope efficiency using

Nd:$YVO_4$ crystal. It is worth mentioning that the value of the *f* function depends on the value of the incident pump power. This dependency has been taken into account in our calculations.

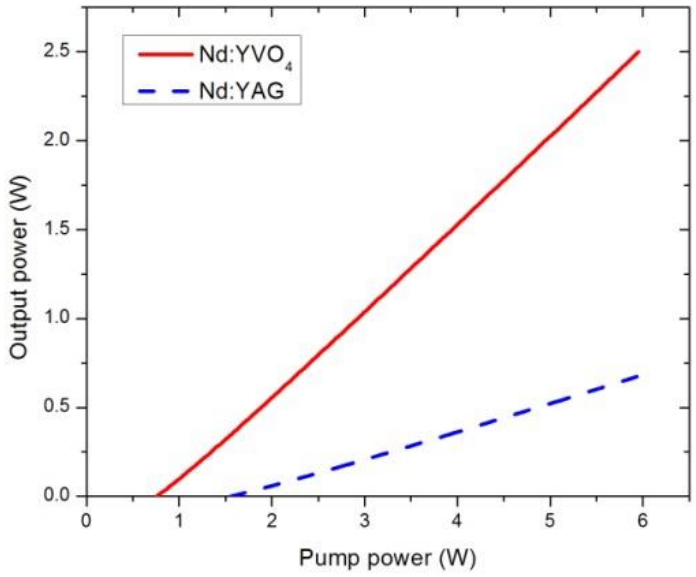


**Figure 3.16 Calculated output power as a function of the pump power for the Nd:YAG and Nd:YVO4 laser crystals pumped by 6 W VCSEL.**

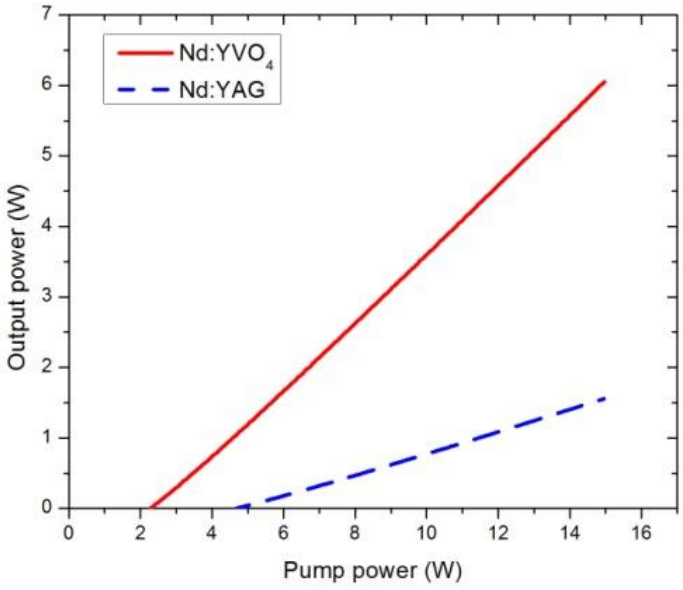


**Figure 3.17 Calculated output power as a function of the pump power for the Nd:YAG and Nd:YVO4 laser crystals pumped by 15 W VCSEL.**

Comparing these two crystals (see figures 3.16, 3.17 and the above discussion), it can be seen that with the same pump beam radius, pump power and crystal length, the Nd:$YVO_4$ crystals pumped by 6 W and 15 W VCSELs will have higher output powers, slope and optical to optical efficiencies. There are several reasons behind this. Firstly, the value of the $\sigma \times \tau$ in the denominator of the threshold pump power expression is higher for the Nd:$YVO_4$ crystal compared to the Nd:YAG crystal [9]. This results in a lower threshold pump power for the Nd:$YVO_4$ (see figures 3.16 and 3.17). Secondly, with a small value for the threshold pump power and the same value for the incident pump power results in a higher value of the *f* function, i.e. in a higher slope efficiency. Thirdly, considering the value of the absorption coefficient, one will have a larger absorption efficiency for the Nd:$YVO_4$ crystal in comparison with the Nd:YAG crystal of the same length. The absorption efficiency of the pump for the 1 mm long Nd:$YVO_4$ and Nd:YAG crystals was calculated to be 79% and 33%, respectively. According to the equation 3.1, a low threshold pump power value and a high slope efficiency will result in a higher output power from the Nd:$YVO_4$ crystal compared to the Nd:YAG.

Equation 3.1 can be also written in another form. By substituting $\eta$ from equation 3.7 into equation 3.1 we get a familiar expression of output power:

$$P_{out} = \eta \times \left(P_{p,inc} - P_{\text{th}}\right) \tag{2.8}$$

As discussed in section 3.2, variation of the *f* function after $P_{p,inc}/P_{th} \cong 10$ becomes very small. Therefore, by increasing the incident pump power high enough above the threshold, the *f* function can be approximated by a fixed value. Considering a fixed pump and laser wavelength and a particular output coupler, the slope efficiency of the output power–pump power characteristic curve described by equation 3.8 then becomes a constant. The linear trend of the

curves in figures 3.16 and 3.17 shows the accuracy of this statement. Table 3.3 shows the summary of the obtained results for the selected working points.

Table 3.3 Summary of the results. Beam waist radii are equal to 0.375 mm and 0.65 mm for the 15 W and 6 W VCSEL modules, respectively.

| | Pump power | Maximum output power | Slope efficiency | Optical to optical efficiency | Depth of focus 10% | Optimum OC |
|---|---|---|---|---|---|---|
| **Nd:$YVO_4$** | 6 W | 2.5 W | 48% | 42% | 2.5 mm | 10% |
| | 15 W | 6 W | 47% | 40% | 4.3 mm | 9% |
| **Nd:YAG** | 6 W | 0.7 W | 16% | 11% | 2 mm | 4% |
| | 15 W | 1.6 W | 15% | 10% | 3.6 mm | 4% |

## 3.6. Conclusions

In conclusion, results of the numerical modeling of longitudinal pumping of the continuous wave (CW) Nd:$YVO_4$ and Nd:YAG lasers by high power VCSEL modules were presented. For Nd:$YVO_4$ crystal, for the 6W VCSEL module, the maximum output power reached 2.5W with a slope efficiency of 48% using a 10% output coupler. In this case the optical-to-optical efficiency was found to be 42%. For the 15W VCSEL module, using a similar output coupler, the maximum output power of 6W was reached with a slope efficiency of 47% and optical-to-optical efficiency of 40%. Comparison with a Nd:YAG showed superior performance of the Nd:$YVO_4$ crystal. Our results therefore indicate that VCSELs can serve as efficient pump sources of the CW Nd:$YVO_4$ lasers. In general, the presented methodology in this work can be thought of as a step by step process of the designing of a CW laser with optimized output power–pump power characteristic curve.

# Chapter 4

# Internal cavity loss measurement

## 4.1 Introduction

Internal cavity loss (i.e. $L_i$) is an important parameter that directly affects laser performance. High internal loss results in a reduced output power, therefore degrading laser efficiency. Knowing the value of the internal cavity loss in a laser cavity would be useful for its optimization [9]. As it was discussed in section 2.5, the Findlay-Clay method is a widely used experimental way of finding the internal cavity loss. However, this method has its own drawbacks.

Implementing the Findlay-Clay method would require replacement of different output couplers. This means that for each output coupler realignment of the cavity would be necessary. This is the first disadvantage of the Findlay-Clay method. In addition, the Findlay-Clay method needs a value of the threshold power for each output coupler. In real situations, the laser would be optimized to get the highest possible power. However, to perform the Findlay-Clay analysis optimization of a laser threshold is needed which usually results in a slightly changed cavity. Moreover, Findlay-Clay analysis returns internal loss values that are obtained at the threshold of laser operation, i.e. not at full output power which is the usual working point of a laser.

In this section, a new method will be introduced. In this method only one measurement in a certain working point of a longitudinally pumped CW laser is required. This means, as opposed to the Findlay-Clay method, that there is no need to do a separate experiment with a changed

cavity optimized only for the threshold. The new method can be performed at any output power of a longitudinally pumped CW laser.

It is worth mentioning that the new method covers all longitudinally pumped lasers while the original article of Findlay-Clay only considered a 4 level gain medium. However, considering the equation derived for the threshold power of all longitudinally pumped CW lasers in the Risk article, the Findlay-Clay method can be revised to be used for all longitudinally pumped CW lasers.

## 4.2 New method for finding internal cavity loss

Let's consider equation 2.54 in section 2.4 again

$$P_{out} \cong \frac{T}{T+L_i} \times \frac{\nu_L}{\nu_P} \times f\left(\frac{P_{\mathrm{p},inc}}{P_{\mathrm{th}}}\right) \times \left(P_{p,abs} - P_{\mathrm{th,abs}}\right) \tag{4.1}$$

In the above equation for an input power and its corresponding measured output power, the internal cavity loss can be found. It is worth mentioning that this equation is valid for a longitudinally pumped CW laser which is oscillating in its fundamental $TEM_{00}$ Gaussian mode.

As can be seen, equation 4.1 depends on the *f* function value. As it was discussed in the previous chapters, the *f* function depends on the overlapping of the pump and laser modes inside the crystal (i.e. *a* parameter, mode size ratio) and also the B parameter. However for a fixed value of the *a* parameter and the B parameter, the *f* is a function of the pump power and threshold power.

In the Risk's article, the pump distribution is considered to be a circular Gaussian beam. Therefore, the calculated *f* function in that work is valid for a CW laser longitudinally pumped by a pump with a circular Gaussian beam distribution (e.g. VCSEL). However in many lasers the pump distribution is much closer to a top-hat beam (e.g. light from fiber-coupled laser diodes). In

the Taira, *et al.* article [7], an expression has been derived for the *f* function for a case that the pump has a top-hat beam distribution.

It is worth mentioning that in the Taira's work [7], a procedure similar to that of the Risk article [6] has been used. The only difference was that the $r_p(r,z)$ was defined for a top-hat distribution as follows:

$$r_p(r,z) = \frac{\alpha}{\eta_a \pi w_p^2} \exp(-\alpha z). \tag{4.2}$$

In Taira's article the above equation was represented in another form:

$$r_p(r,z) = \frac{\alpha l_c^*}{2\eta_a \pi w_p^2} \exp(-\alpha z), \tag{4.3}$$

where $l_c^*$ is the cavity's optical path length defined as [7]

$$l_c^* = l_c + (n-1)l, \tag{4.4}$$

and where $l_c$ is the cavity length. As it was defined in Chap.2, $n$ and $l$ are the refractive index and the length of the gain medium, respectively.

To generate the *f* function for a 4 level laser (*B=0*) pumped by a beam with a top-hat intensity distribution, equations 4.5 and 4.6 (equation 18 and 14 respectively in the reference [7]) were numerically solved together.

$$\frac{dS}{dF} = \frac{2\left[1+\frac{B}{S/C}\ln(1+S/C)\right]}{(F/C)\left\{(F/C)\int_0^2 \frac{\exp(-2a^2x)}{\left[1+(S/C)\exp(-a^2x)\right]^2}dx - 2Ba^2\int_0^\infty \frac{\exp(-2a^2x)}{\left[1+(S/C)\exp(-a^2x)\right]^2}dx\right\}}, \tag{4.5}$$

$$\frac{F}{C} = \frac{2\left[1+\frac{B}{S/C}\ln(1+S/C)\right]}{\int_0^2 \frac{\exp(-a^2x)}{1+(S/C)\exp(-a^2x)}dx}, \tag{4.6}$$

where C parameter was defined as

$$C = \frac{\pi w_L^2 l_c^*}{2}, \tag{4.7}$$

and this parameter is a normalized factor for laser photon distribution in the cavity. Figure 4.1 shows the results for *a*=1, 1.1 and 1.2. As can be seen from the figure 4.1, a dramatic change in the *f* function occurs when the pump power is around the threshold.

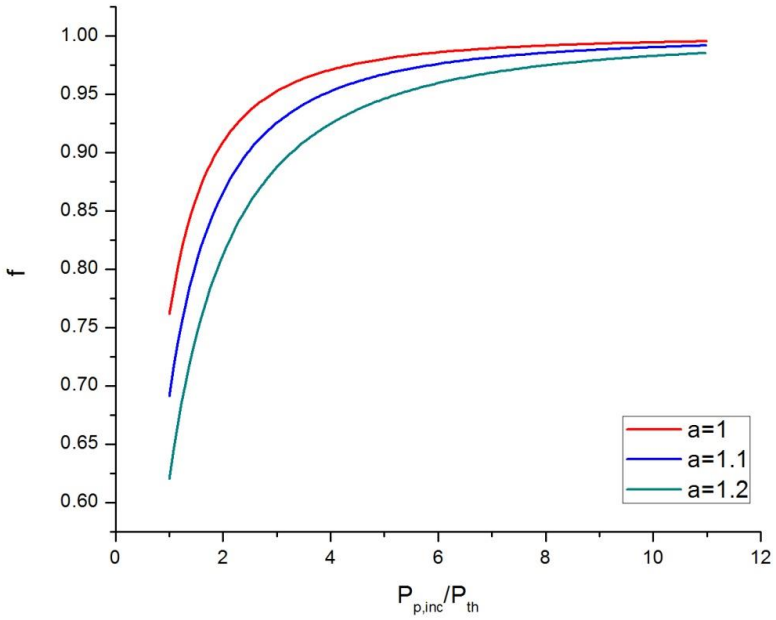


Figure 4.1 Calculation of the $f$ in a 4 level laser as a function of Pp,inc/Pth for different a values

To see the difference between the *f* function of a Gaussian pump and a top-hat pump, both *f* functions were plotted for a fixed B and *a*. Figure 4.2 shows a comparison between the calculated *f* functions for a 4 level laser (i.e. B=0) with a=1when the pump has the Gaussian distribution (blue line) and the top-hat distribution (red line). As can be seen, the *f* function for the top-hat pump has a more dramatic change near the threshold compared to that one of the Gaussian pump.

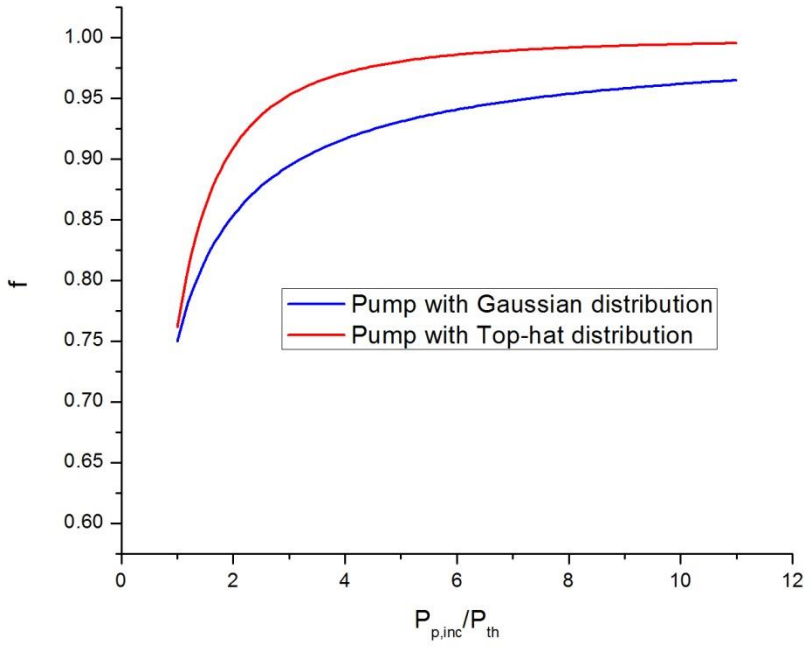


Figure 4.2 Comparison of the f function for the top-hat and Gaussian pump beam distributions with a=1 in a four level laser

## 4.3 Experimental results

In this section, the new method and the Findlay-Clay method will be practically investigated in a diode-pumped Nd:$YVO_4$ laser. Therefore, a laser was designed for an internal cavity loss measurement. Then, the Findlay-Clay method and the new method were performed and compared.

### 4.3.1 Laser cavity and measurements

A laser cavity was designed to have an equal pump beam waist and a laser beam waist along the length of a gain medium. Figure 4.3 shows a schematic of the designed cavity. The gain medium used in this work was Nd:$YVO_4$ crystal which is a 4 level medium (i.e. B=0). The gain medium

used in this work was a 0.5% doped and a-cut crystal with the length of 12 mm and cross section of 3×3 $mm^2$. The water cooling system positioned on the top and bottom of the crystal, kept its surface at 16˚C. Moreover, the cavity was designed such that the changes in the thermally induced lens inside the gain medium did not affect the laser beam overlap inside the gain medium. The investigated Nd:$YVO_4$ laser had a thermal lens ranging from approximately 800 mm (at about 5 W of pump power) to 500 mm (at about 9W of pump power) [27].

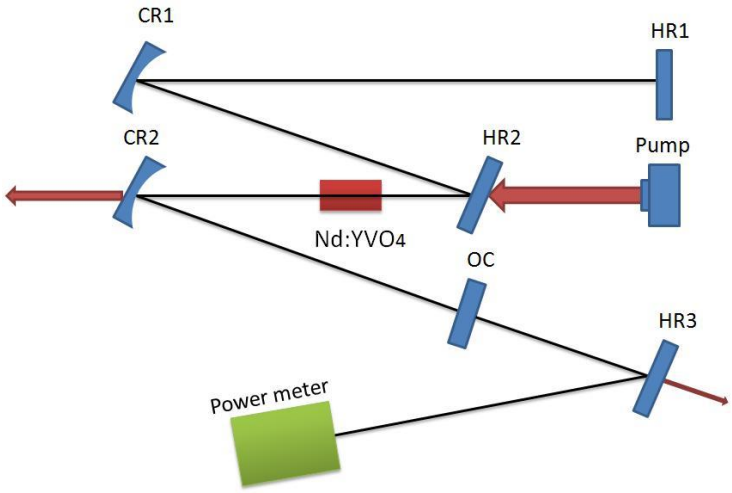


Figure 4.3 Experimental setup

As can be seen in the figure 4.3, we have three curved mirrors (i.e. CR1, CR2 and HR3).The HR2 mirror reflects the laser beam but lets the pump pass through. It is worth mentioning that the main part of the pump power after exciting the gain medium will leave the cavity from the CR2. However, to remove any possible residual pump another mirror similar to HR2 has been used (HR3).

The pump was a fiber-coupled laser diode. Since the pump was fiber-coupled, its beam distribution was closer to the top-hat. In addition, the wavelength of the pump changed with the input current. This means that by increasing the pump power, the wavelength of the pump increased. Our practical test showed the change of the pump wavelength from around 905 nm to 914 nm when the power was increased from 1W to 17 W.

The electrical power supply used for feeding the pump had a fixed voltage and a variable current. The minimum increment step and maximum current value of the current supply were 100 mA and 10 A respectively. Since in the equation 4.1 the absorbed input power is used, two experiments were conducted to find out the absorbed power by the crystal for different pump powers. The first experiment was conducted to determine the absorbed pump power by the crystal for different pump input current levels (see figure 4.4(a)).In addition, another separate experiment was conducted for conversion of the pump diode's input current to the absorbed pump power by the crystal. Figure 4.3(b) shows the result of this conversion. Although the same input current values were used in both experiments, there is an uncertainty of ±100mA in all measured points due to the accuracy of the current supply. As can be seen, the graphs are not linear as expected. Considering dramatic variation of the absorption cross section of the Nd:$YVO_4$ around 914 nm, the pump diode's wavelength shift with increasing output power was the main reason that caused the obvious nonlinearity of the graphs. Therefore, the data presented in figure 4.4 should be considered as only approximate relationships between the diode's current, output and the absorbed powers. Because of the number of different effects involved it is difficult to put a specific error bar on these measurements. The lasing wavelength of the laser was 1064 nm.

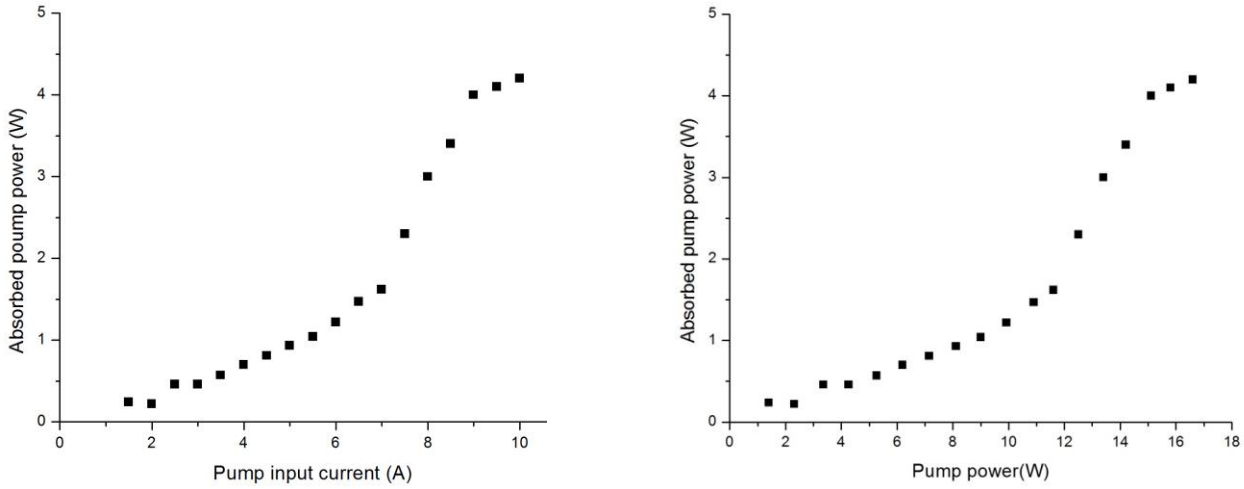


(a) (b)

Figure 4.4 (a) Absorbed power (W) by gain medium as a function of pump input current (A) (b) Absorbed power (W) by gain medium as a function of pump power (W)

### 4.3.2 Findlay-Clay method

Accurate measurement of the threshold pump power is a critical step in the Findlay-Clay method. Therefore, spectrometer and a sensitive florescence card have been used to detect the threshold power. Practically when blinking of the laser was seen we accepted this value of the pump power as the threshold power.

As it was discussed in section 2.5 of Chap.2, in the Findlay-Clay method the threshold pump power for different output couplers should be measured. A plot of –ln(R) versus $P_{th}$ is made. Then by drawing a trend line the internal cavity loss can be found at the intercept with the –ln(R) axis. Figure 4.5 shows the measurement results (black dots) and the calculated trend line (red line).

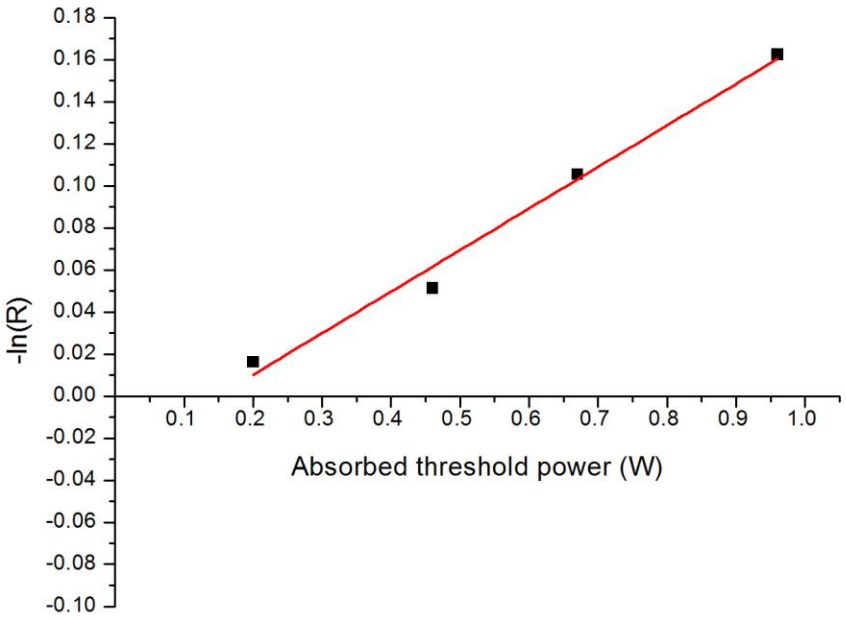


Figure 4.5 Findlay-Clay method

It should be mentioned that measured values of the absorbed threshold power in the figure 4.5 have an uncertainty cussed by the conversion of the input pump current to the absorbed pump power.

The trend's line equation is y= 0.19761x-0.0293, where x and y are horizontal and vertical axes that correspond to the plotted -ln(R) and $P_{th}$ values. Therefore, the internal cavity loss according to the Findlay-Clay method can be found as 2.93%.

### 4.3.3 New method

The maximum absorbed pump power which could be obtained in the experiment was 4.2 W. The designed laser cavity with 1.6% output coupler was optimized at the maximum pump power to get the highest output power which was 1.3W as shown in Fig 6. It is worth mentioning that the

optimized cavity had the threshold pump power of 3W. Let's consider the highest output power as a working point for finding the internal cavity loss using the new method.

The pump had a beam with top-hat distribution. Therefore, considering the calculated *f* functions in the section 4.2, the one for the top-hat pump and a 4 level gain medium (where B=0 and a =1) should be selected (i.e. the red line in figure 4.1). Considering equation 4.1, all parameter and the *f* function are known at the working point. Therefore, the internal cavity loss value was found using the new method to be 2.4%. As can be seen, the Findlay- Clay method and the new method have almost the same result for this working point.

### 4.3.4 Investigation of the new method

In the previous section, the internal cavity loss parameter was found using both the Finlay- Clay and the new method. In this section the determined value for the $L_i$ parameter will be used in the longitudinally pumped CW laser model for comparison with experimental results.

In the figure 4.6 the black dots show the measured output power values versus the input pump power of the laser with 1.6 % output coupler when it was optmized to get the highest output power. It is worth mentioning that the optimization was done at the highest absorbed pump power. As can be seen, the black dots don't have a linear trend as expected. The reason behind this is the nonlinear variation of the absorbed pump power (see figure 4.4(a) and 4.4(b)) caused by the pump wavelength shifts with the pump power.

The lines in figure 4.6 show the calculated trends based on the equation 4.1.The threshold value used in the calculations was measured to be 3W. The red line shows the modeling result when $L_i$ was calculated using the new method. The highest absorbed power was used as a working point for the internal cavity loss calculation. The blue line is also the modeling result based on equation 4.1 and the measured threshold pump power but the $L_i$ parameter which was used in the

calculation was found from the Findlay-Clay method (see section 4.3.2 ). It is worth mentioning that the *f* fuction which was used for finding the red and blue lines was calculated for the top-hat pump, 4 level gain medium (B=0 ) and a =1 (i.e. red line in figure 4.1).

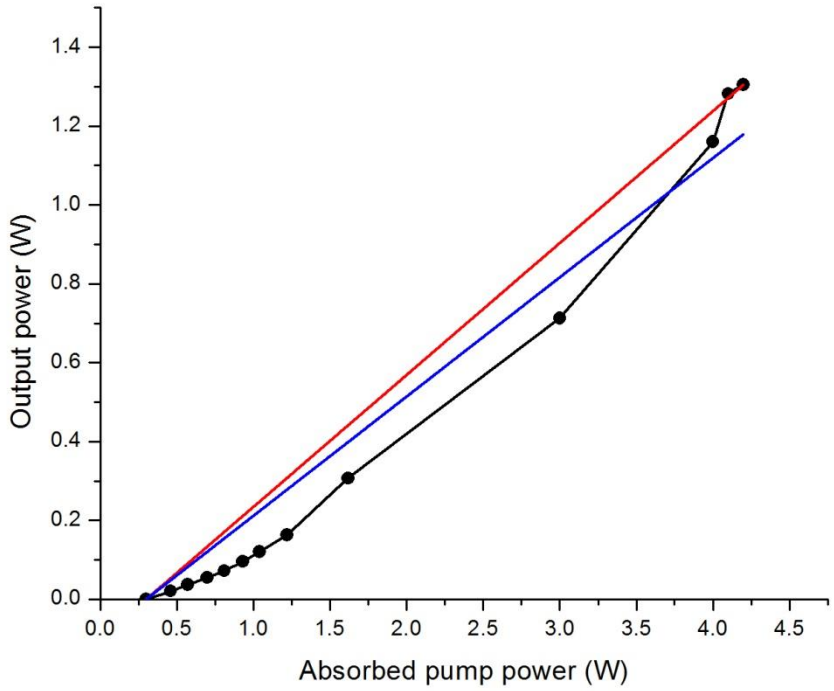


**Figure 4.6 Black dots are the measured output power values. The red line is the calculated output power in which the $L_i$ was calculated from the new method. The blue line is the calculated output power in which the $L_i$ was calculated from the Findlay-Clay method.**

It is worth mentiong that the recorded values for the absorbed pump power used in the caclulation of the $L_i$ with the help of the new method and figure 4.6 have an uncertainty due to the conversion of the pump input current to the absorbed pump power as was explained earlier in section 4.3.1.

For further investigation of the new method, the internal cavity loss for different measured working points was calculated using this method. The measured working points are absorbed pump powers and their corresponding measured output powers shown in figure 4.6. In figure 4.7

the black squares show the calculated values for the internal cavity loss for each working point. Working points in figure 4.7 are represented by the absorbed pump power and can be linked to the corresponding output power with the help of figure 4.6.

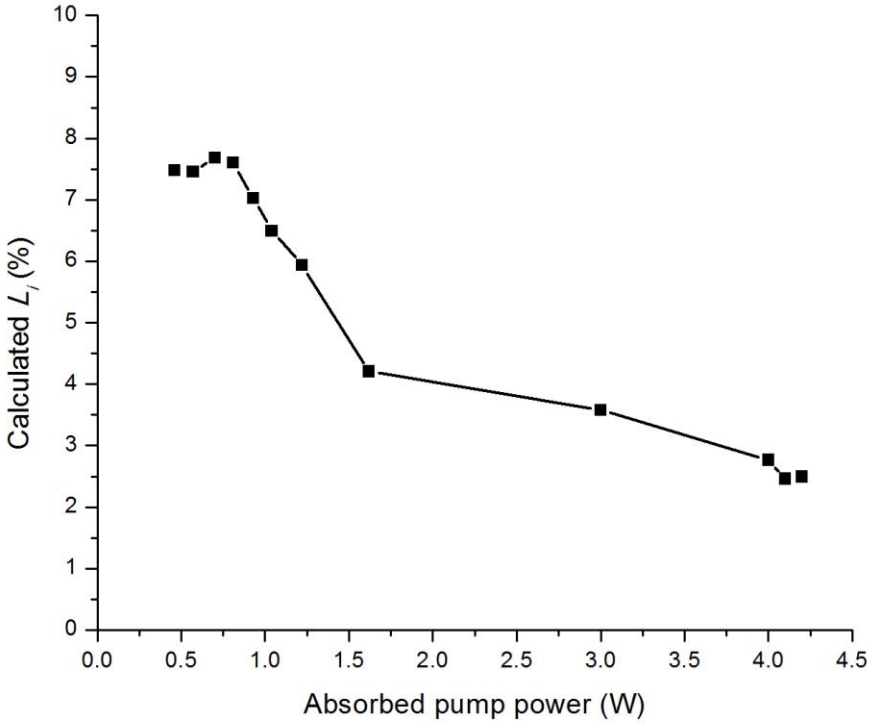


Figure 4.7 Calculation of the internal cavity power for all measured points

As can be seen from figure 4.7 the value of the internal cavity loss changes for different working points. The value of the internal cavity loss is 2.4% at the highest absorbed pump power and about 7.5% around the threshold. This significant change of the calculated internal cavity loss for different working points is not reasonable and can be explained by the uncertainty in the relationship between the absorbed pump and the laser output powers (see figure 4.4).

Additional errors that could have come from the gain medium itself could be caused by the thermal lens of the Nd:$YVO_4$ and pump saturation at the higher pump power levels. Possible double pass of the pump through the gain medium can be also counted as a laser cavity error.

In our calculations, the variation of the pump wavelength with the diode's current was neglected and was assumed to be 914 nm.

In the design of the cavity, the thermally induced lens in the gain medium was taken into account and also in the measurement a time period of 2 minutes was allowed for stabilization of the laser. However, due to the presence of thermal lens this timing can affect the final result.

## 4.4 Conclusions and future work

In this work a new method of determining the internal cavity loss for longitudinally pumped CW lasers was introduced. An experiment was conducted for comparing the Findlay-Clay method with the new method and the sources of possible error in the internal cavity loss measurement were discussed.

In the new method, having one set of output power data at any absorbed pump power level and the pump threshold value are the only measured data that are required for the calculation of the internal cavity loss. As opposed to the Findlay-Clay method there is no need to change the output couplers in the cavity and re-do the alignment of the laser to find out the internal cavity loss.

The conducted measurements have some error sources coming from the pump and the gain medium, and the laser cavity design. These errors can be caused by wavelength shift of the pump, measurement of the residual pump in addition to the real laser output power, thermal lensing in the gain medium.

In future work, the discussed errors can be better managed or to be removed. For example, since the wavelength shift of the VCSEL is more controllable compared to that of the edge emitting laser diodes used in this work, VCSELs will be the good candidates to remove the pump errors in the measurement. The measurement setup should be designed in a way that the double pass of the pump is eliminated and the residual pump is removed.

# Chapter 5

## Conclusions and future works

The core of this thesis was application of the Risk model for longitudinally pumped continuous wave lasers. The model was used for a numerical study of a CW operation of Nd:$YVO_4$ laser longitudinally pumped by high power VCSEL modules. In addition, based on the model a new experimental method for determination of the internal cavity loss ($L_i$) value was introduced. It is worth mentioning that the methodology used in Chap.3 can be considered as a step by step design process for an optimized longitudinally pumped CW laser given that the parameters of the pump are known.

This work started with detailed explanation of the model and the Findlay-Clay method. In addition, VCSEL was explained and proposed to be used for longitudinal pumping of a CW laser.

In this study, Nd:YAG and Nd:$YVO_4$ gain media were compared as possible candidates to be longitudinally pumped by the VCSEL modules. Two commercially available VCSEL pump modules (6 W and 15 W) were compared as a pump source for the end-pumped CW lasers. The maximum output power from a Nd:$YVO_4$ crystal using these pump modules was calculated to be 2.5 W and 6 W, respectively, using a 10 % output coupler. The slope and optical-to-optical efficiencies in both cases were around 47% and 40%, respectively. The performance of Nd:YVO4 crystal was found to be better than that of a Nd:YAG crystal. Our numerical results indicate that VCSELs can serve as efficient pump sources for the end-pumped CW Nd:$YVO_4$ lasers.

In future, the methodology introduced in Chap.3 can be used universally. For this purpose a software tool can be developed for determination of the required pump, gain medium and the output coupler for a certain end-pumped CW laser characteristics. For instance, characteristics such as threshold power, slope and optical-to-optical efficiencies and maximum output power would be given to the software as inputs and it would return the pump parameters (such as N.A. and $M^2$), gain medium parameters (from a predefined list) and its optimum length, and an optimum output coupler with acceptable value of the internal cavity loss.

In future, a CW laser which is optimized through the provided methodology in this study can be experimentally studied. In addition, VCSEL can be experimentally tested for the longitudinal pumping of an optimized CW laser. This optimized laser pumped by a VCSEL can be used as a starting point for building of the efficient mode-locked and Q-switched lasers.

In addition, in this work a new method for determining the $L_i$ value in a longitudinally pumped CW laser was introduced and compared with the Findlay-Clay method. An experiment was conducted for finding of the $L_i$ of a diode-pumped laser using both methods. The experimental errors introduced by the pump, gain medium and laser cavity were discussed in details.

The errors in the internal cavity loss measurement discussed in Chap.4 can be removed in new experiments. More controllable wavelength shift of the VCSELs compared to that of the edge emitting laser diodes makes them a good candidate for removing pump errors from the experiment.

The pump distribution in the Risk model is assumed to be an ideal Gaussian, however in a real situation the pump distribution is a Gaussian with a certain $M^2$. This means that the pump distribution have a deviation from that of an ideal Gaussian. This assumption can be thought of

as a source of error in the agreement of the model with experimental results. Therefore, in future, considering the same method used in the Risk's model, a new equation for generating of the $f$ function based on a pump distribution with a certain $M^2$ can be derived for the longitudinally pumped CW lasers.

In addition, in the Risk's model, the ratio of a pump beam waist to a laser beam waist (i.e. $a$) is not space dependent parameter. However, in a real situation due to having different $M^2$ factors for the laser and pump beam distributions, this ratio is a space dependent parameter. Although the defined 10% confocal parameter can solve the problem for many cases, a new, more general model for longitudinally pumped CW lasers can be proposed in future for more accurate results.

# Chapter 6

# Bibliography

[1] Alimohammadian, E., & Major, A. "Modeling of a CW Nd:$YVO_4$ laser longitudinally pumped by high power VCSEL modules at 808 nm", in Solid State Lasers XXIII: Technology and Devices, Photonics West 2014, February 1-6, San Francisco, USA, oral

[2] Alimohammadian, E., & Major, A. (2014). Modeling of a CW Nd:$YVO_4$ laser longitudinally pumped by high power VCSEL modules at 808 nm. Proc. SPIE, Vol. XYZ, pp. 89591D-89591D-10.

[3] Saleh, B. E., & Teich, M. C. Fundamentals of photonics. 2007.

[4] Goldsmith, P. F., Institute of Electrical and Electronics Engineers & Microwave Theory and Techniques Society. (1998). Quasioptical systems: Gaussian beam quasioptical propagation and applications. IEEE press, New York.

[5] Novotny, L., & Hecht, B. (2012). Principles of nano-optics Cambridge university press.

[6] Risk, W. (1988). Modeling of longitudinally pumped solid-state lasers exhibiting reabsorption losses. JOSA B, 5(7), 1412-1423.

[7] Taira, T., Tulloch, W. M., & Byer, R. L. (1997). Modeling of quasi-three-level lasers and operation of cw Yb: YAG lasers. Applied Optics, 36(9), 1867-1874.

[8] Alfrey, A. J. (1989). Modeling of longitudinally pumped CW Ti: sapphire laser oscillators. Quantum Electronics, IEEE Journal of, 25(4), 760-766.

[9] Koechner, W. (2006). Solid-state laser engineering (Vol. 1). Springer.

[10] Kay, R. B., & Poulios, D. (2005). Q-switched rate equations for diode side-pumped slab and zigzag slab lasers including Gaussian beam shapes. Quantum Electronics, IEEE Journal of, 41(10), 1278-1284.

[11] Svelto, O. (2010). Principles of Lasers. Springer.

[12] Findlay, D., & Clay, R. A. (1966). The measurement of internal losses in 4-level lasers. Physics Letters, 20(3), 277-278.

[13] Soda, H., Iga, K. I., Kitahara, C., & Suematsu, Y. (1979). GaInAsP/InP surface emitting injection lasers. Japanese Journal of Applied Physics, 18(12), 2329.

[14] Michalzik, R. (2013). Fundamentals, Technology and Applications of Vertical-Cavity Surface-Emitting Lasers. Springer.

[15] Sands, D. (2010). Diode lasers. CRC Press.

[16] Jewell, J. L., Lee, Y. H., Harbison, J. P., Scherer, A., & Florez, L. T. (1991). Vertical-cavity surface-emitting lasers-design, growth, fabrication, characterization. IEEE Journal of Quantum Electronics, 27, 1332-1346.

[17] Lei, C., Rogers, T. J., Deppe, D. G., & Streetman, B. G. (1991). ZnSe/CaF2 quarter-wave Bragg reflector for the vertical-cavity surface-emitting laser. Journal of Applied Physics, 69(11), 7430-7434.

[18] Huffaker, D. L., Deppe, D. G., Kumar, K., & Rogers, T. J. (1994). Native-oxide defined ring contact for low threshold vertical-cavity lasers. Applied Physics Letters, 65(1), 97-99.

[19] Young, D. B., Scott, J. W., Peters, F. H., Peters, M. G., Majewski, M. L., Thibeault, B. J., ... & Coldren, L. A. (1993). Enhanced performance of offset-gain high-barrier vertical-cavity surface-emitting lasers. Quantum Electronics, IEEE Journal of, 29(6), 2013-2022.

[20] Seurin, J. F., Xu, G., Khalfin, V., Miglo, A., Wynn, J. D., Pradhan, P., ... & D'Asaro, L. A. (2009, February). Progress in high-power high-efficiency VCSEL arrays. In Proc. SPIE (Vol. 7229, p. 722903).

[21] Van Leeuwen, R., Xiong, Y., Seurin, J. F., Xu, G., Miglo, A., Wang, Q., ... & Ghosh, C. L. (2012, May). High-power vertical-cavity surface-emitting lasers for diode pumped solid-state lasers. In SPIE Defense, Security, and Sensing (pp. 83810I-83810I). International Society for Optics and Photonics.

[22] Goldberg, L., McIntosh, C., & Cole, B. (2011). VCSEL end-pumped passively Q-switched Nd: YAG laser with adjustable pulse energy. Optics Express, 19(5), 4261-4267.

[23] Van Leeuwen, R., Xiong, Y., Watkins, L. S., Seurin, J. F., Xu, G., Wang, Q., & Ghosh, C. (2011, February). High power 808 nm VCSEL arrays for pumping of compact pulsed high energy Nd: YAG lasers operating at 946 nm and 1064 nm for blue and UV light generation. In SPIE LASE (pp. 79120Z-79120Z). International Society for Optics and Photonics.

[24] Turri, G., Jenssen, H. P., Cornacchia, F., Tonelli, M., & Bass, M. (2009). Temperature-dependent stimulated emission cross section in $Nd^{3+}$:$YVO_4$ crystals. JOSA B, 26(11), 2084-2088.

[25] Demidovich, A. A., Shkadarevich, A. P., Danailov, M. B., Apai, P., Gasmi, T., Gribkovskii, V. P., ... & Batay, L. E. (1998). Comparison of cw laser performance of Nd: KGW, Nd: YAG, Nd: BEL, and Nd: $YVO_4$ under laser diode pumping. Applied Physics B, 67(1), 11-15.

[26] Taira, T., Mukai, A., Nozawa, Y., & Kobayashi, T. (1991). Single-mode oscillation of laser-diode-pumped Nd:$YVO_4$ microchip lasers. Optics Letters, 16(24), 1955-1957.

[27] Waritanant, T., & Major, A. (2014, June). Thermal Lensing in Nd:$YVO_4$ Laser with In-Band Pumping at 914 nm. In CLEO: QELS_Fundamental Science (pp. JTh2A-80). Optical Society of America.